Biotechnology, Chemical and Materials Engineering II

Edited by
Wen-Pei Sung, Chun-Zhi Zhang and Ran Chen

TRANS TECH PUBLICATIONS

Biotechnology, Chemical and Materials Engineering II

Edited by
Wen-Pei Sung
Chun-Zhi Zhang
Ran Chen

Biotechnology, Chemical and Materials Engineering II

Selected, peer reviewed papers from the
2012 The 2nd International Conference on
Biotechnology, Chemical and Materials Engineering
(CBCME 2012),
December 28-29, 2012, Xiamen, China

Edited by

Wen-Pei Sung, Chun-Zhi Zhang and Ran Chen

TTP

Trans Tech Publications Ltd
Kreuzstrasse 10
CH-8635 Durnten-Zurich
Switzerland
http://www.ttp.net

Volumes 641-642 of
Advanced Materials Research
ISSN print 1022-6680
ISSN cd 1022-6680
ISSN web 1662-8985

Full text available online at *http://www.scientific.net*

***Distributed** worldwide by*

Trans Tech Publications Ltd
Kreuzstrasse 10
CH-8635 Durnten-Zurich
Switzerland

Fax: +41 (44) 922 10 33
e-mail: sales@ttp.net

and in the Americas by

Trans Tech Publications Inc.
PO Box 699, May Street
Enfield, NH 03748
USA

Phone: +1 (603) 632-7377
Fax: +1 (603) 632-5611
e-mail: sales-usa@ttp.net

Preface

2012 International Conference on Biotechnology, Chemical and Materials Engineering (CBCME 2012) will be held in Xiamen, China during December 28-29, 2012. CBCME 2012 is sponsored by Hong Kong Control Engineering and Information Science Research Association (CEIS), Dalian Polytechnic University, International Frontiers of Science and Technology Research Association (IFST) and Trans tech publications inc. The aim is to provide a platform for researchers, engineers, academicians as well as industrial professionals from all over the world to present their research results and development activities in Biotechnology, Chemical and Materials Engineering.

In this conference, we received more than 700 submissions from email and electronic submission system, which were reviewed by international experts, and about 223 papers have been selected for presentation, representing 9 national and international organizations. This high level of interest truly reflects the worldwide importance of Biotechnology, Chemical and Materials Engineering.

I think that CBCME 2012 will be the most comprehensive Conference focused on the Biotechnology, Chemical and Materials Engineering. The conference will promote the development of Biotechnology, Chemical and Materials Engineering, strengthening the international academic cooperation and communications, and exchanging research ideas.

We would like to thank the conference chairs, organization staff, the authors and the members of International Technological Committees for their hard work. Thanks are also given to Trans Tech Publications.

We hope that CBCME 2012 will be successful and enjoyable to all participants. We look forward to seeing all of you next year at the CBCME 2013.

November, 2012

Conference Chairman

Wen-Pei Sung
Wen-Pei Sung, National Chin-Yi University of Technology

Chun-Zhi Zhang
Dalian Polytechnic University

Ran Chen
Control Engineering and Information Science Research Association

CBCME 2012 Committee

Conference Chairman

Wen-Pei Sung, National Chin-Yi University of Technology
Chun-Zhi Zhang Dalian Polytechnic University
Chen Ran, Control Engineering and Information Science Research Association

Program Committee

Hsien-Te Lin, National Cheng Kung University
Xue Chaogai, Zhengzhou University, China
Viranjay M.Srivastava, Jaypee University of Information Technology, Solan, H.P. ,India
Zhao Weiguo, Hebei University of Engineering, China
He Qing, North China Electric Power University, China
Mir Mahdi Zalloi, Iron
Zhou Liang, Donghua University, China
Liu Yunan, University of Michigan, USA
Wang Liying, Institute of Water Conservancy and Hydroelectric Power, China
Chenggui Zhao, Yunnan University of Finance and Economics, China
Hsiang-Chuan Liu, Asia University
Gang Shi, Inha University, South KoreaBhagavathi Tarigoppula, Bradley University, USA
Tjamme Wiegers, Delft University of Technology, Netherlands
Anita Kovač Kralj, University of Maribor, Slovenia
Wei Fu, Chongqing University, China
Ramezan ali Mahdavinejad, University of Tehran, Iran
Chen Chi-Hua, National Chiao Tung University
Mostafa Shokshok, National University of Malaysia, Malaysia
Hong Sheng, Beijing University of Aeronautics and Astronautics, China
Yang Yan, Guangxi University for Nationalities, China
Xu Chungeng, Nanjing University of Science and Technology, China
Liu Zheng, Shangdong Economic University, China
Wen-Sheng Ou, National Chin-Yi University of Technology
Hao-En Chueh Yuanpei University
Li Zhong, North China Electric Power University, China
Lixin Guo, Northeastern University, China

Co- Sponsor

Dalian Polytechnic University
International Frontiers of science and technology Research Association
HongKong Control Engineering and Information Science Research Association
Trans tech publications inc.

Table of Contents

Chapter 2: Applications of Materials in Manufacturing Technologies, Materials Science and Engineering

Chapter 3: Biochemical, Medicine Engineering and Technoligies, Applications of Genetic Engineering

CHAPTER 1:
Environmental Chemistry, Chemical Manufacturing, Technologies and Engineering

Advanced Materials Research Vols. 641-642 (2013) pp 3-6

doi:10.4028/www.scientific.net/AMR.641-642.3

Comparative Researches on Two Kinds of Staining Method of Acetylcholinesterase Isozymes

Gan Zhao[1 a], Kangjie Chen[2,b] , Shaocong Wu[3,c] ,Qinchuan Zhuang[4,d], Fang Qian[5,e]

[1.] College of Life Science , South China Agricultural University , Guangzhou 510642 , China ;
[2-4.] College of Science , South China Agricultural University , Guangzhou 510642 , China ;
[5.] College of Nursing , Guangzhou Medical College, Guangzhou 510180 , China

[a, *]E-mail: Corresponding Author, zg200010@163.com.
[b]E-mail: chenkangjie08@163.com , [c]E-mail: 328559049@qq.com,
[d]E-mail: 106704796@qq.com, [e]E-mail: qqianffang@sina.com

Keywords: acetylcholinesterase, isozyme, staining method , $K_3[Fe(CN)_6$, $CuSO_4$, $FeCl_3$;

Abstract: The staining effects of two staining methods of acetylcholinesterase isozymes were compared . One using acetylthiocholine iodide , $K_3[Fe(CN)_6]$ and $CuSO_4$ was named as AFCu method, and the other one using acetylthiocholine iodide , $K_3[Fe(CN)_6]$ and $FeCl_3$ was named as AFFe method. The staining effect of former was better.

By physiological researches the acetylcholinesterase (AChE,EC. 3.1.1.7), xisting in red cells, liver, spleen, nerve and muscle, plays an important role in erveconduction processes in lives[1]. For its close relationships with Alzheimer's disease (AD), close attention to the function of the AChE in the formation and development of lzheimer's disease[2] and the screen of its inhibitors [1,3,4]have been paid in the academic world. Otherwise, to meet the need of rapid detection of organophosphorus pesticides and monitoring of environmental pollution [1,5], the AChE has also become more and more important.Two staining methods of AChE isozymes will be compared ,in order to be helpful to the researches on the AChE .

Because the cholinesterase in the serum is called butyrylcholin-esterase (EC 3.1.1.8) , which can also use ATCI as its substrate [6],the pig serum was used to compare the both staining methods of isozymes of AChE here.

1. Material ,reagents and instruments

Fresh pig blood was got from a slaughterhouse. S-acetylthiocholine iodide（ATCI）was from Alfa Aesar Company in Tianjin in China. 5,5'-Dithiobis(2-nitrobenzoic acid) (DTNB)was from Shanghai Bo'ao Biological Technology Co., Ltd. in China.Other biochemical or analytical reagents are made in China .

752 Type -Ultraviolet Grating Spectrophotometer was made by Shanghai Accurate Scientific Instruments Corporation. HWS24 Type Electro-thermal Constant Temperature Water Bath was made by Shanghai Yiheng Technology Corporation. HF-200Type Electronic Balance was made by A&D Company，limited. DYY-5 Steady Voltage and Steady Flow Electrophoresis was made by Beijing Liuyi Instrument Factory. 5810(R) High-speed Refrigerated Centrifuge was made by Eppendof China Ltd..

2. Experimental methods

2.1 Preparation some solution

2.1.1 Incubation Solution A ：18ml of Tris-HCl buffer（pH 8.0,0.05 mol/L）was mixed with 0.16 ml of 4%(m/V) ATCI solution fully.It was used freshly .

2.1.2 Incubation Solution B ： 18ml of DDW was mixed with 0.16 ml of 4%(m/V) ATCI solution and 2.5 ml of 0.825％ (m/V) $K_4[Fe(CN)_6]$ solution fully.It was used freshly .

2.1.3 Staining Solution A ：18ml of Tris-HCl buffer （pH 8.0,0.05 mol/L）was mixed with 2.5 ml of 3.3%(m/V) $K_4[Fe(CN)_6]$ solution and 2.5 ml of 0.75％%(m/V) $CuSO_4$ solution fully.It was used freshly .

2.1.4 Staining Solution B ： 18ml of DDW was mixed with 2.5 ml of 0.75％%(m/V) $FeCl_3$ solution fully.It was used freshly .

2.2 Treatment of pig serum

The fresh pig blood was placed for a while at room temperature, then was centrifuged at 4000 rpm for 10 min at 4℃. The supernatant collected was the pig serum,which could be placed in the refrigerator at 4℃ . 30ml of PBS（pH7.2，0.05mol/L）was mixed with 10ml of pig serum, to get the precipitate during 55％-70％ saturation of $(NH_4)_2SO_4$ at 4℃ by salting out. The precipitate was dissolved in DDW and was used as AChE experimental sample after dialysis .

2.3 The AChE isozyme were separated by PAGE, according to the methods [7].

2.4 The AChE isozymes were stained by the methods introduced below.

A. Staining method with ATCI , $K_4[Fe(CN)_6]$ and $CuSO_4$ solution:

After PAGE, the gel with the separated AChE isozymes sample was soaked in the freshly prepared incubation solution A for 1 hr at 4℃. Then the gel ,after being washed for 2 times with DDW, was soaked in the freshly prepared staining solution A overnight. Finally the gel ,after being washed for 2 times with DDW, was soaked in DDW ,to have a photo taken. This method was named as AFCu method .

B. Staining method with ATCI , $K_4[Fe(CN)_6]$ and $FeCl_3$ solution:

After PAGE, the gel with the separated AChE isozymes sample was soaked in the freshly prepared incubation solution B for 1 hr at 4℃. Then the gel ,after being washed for 2 times with DDW, was soaked in the freshly prepared staining solution B overnight. Finally the gel ,after being washed for 2 times with DDW, was soaked in DDW ,to have a photo taken. This method was named as AFFe method .

3. Results and Discussion

From Fig. 1, the AChE isozymes, existing in the separated pig serum and enzyme samples ,could be stained as 4 bands and 2 bands of clear brown by AFCu method. The background of the gel was very light ,easy to be observated and have a photo taken.From Fig. 2 , the AChE isozymes, existing in the separated pig serum and enzyme samples ,could also be stained as 4 bands and 2 bands of blue by AFFe method, but the background of the gel was very dark and the bands were not clear sufficiently, difficult to be observated and have a photo taken. So the AFCu method was more sensitively than the AFFe method to stain the AChE isozymes to be used to detect the AChE isozymes, and so on.

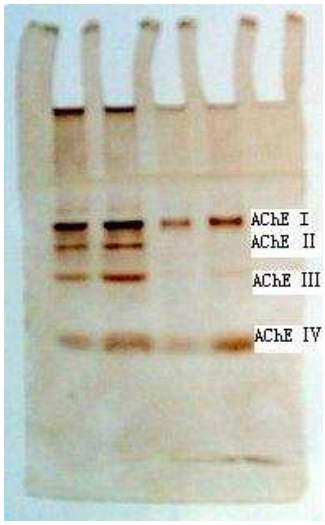

1 2 3 4

1. 5μL pig serum; 2.10μL pig serum;
3. 5μL enzyme sample; 4.10μL enzyme sample ;

Fig.1:Zymogram of acetylcholinesterase stained by the method withATCI, $K_3[Fe(CN)_6]$and $CuSO_4$ (or AFCu method)

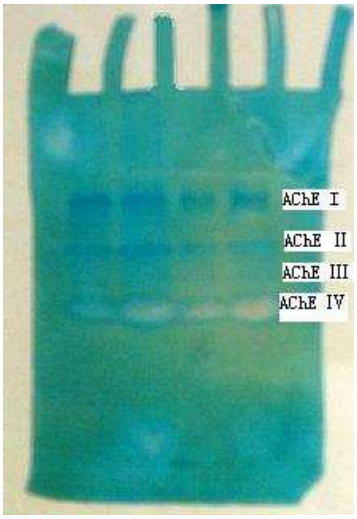

1 2 3 4

1. 5μL pig serum; 2.10μL pig serum;
3. 5μL enzyme sample; 4.10μL enzyme sample;

Fig.2: Zymogram of acetylcholinesterase stained by the method with ATCI, $K_3[Fe(CN)_6]$and $FeCl_3$ (or AFFe method)

In the both methods, acetylthiocholine iodide was all at first hydrolysed to produce acetic acid and thiocholine iodide by the AChE. The potassium ferricyanide ($K_3[Fe(CN)_6]$) was reduced by the thiocholine produced ,changing into potassium ferrocyanide ($K_4[Fe(CN)_6]$) . Then in the AFCu method, the $K_4[Fe(CN)_6]$ produced could react with $CuSO_4$ producing the brown deposit cupric ferrocyanide ($Cu_2[Fe(CN)_6]$), which once was used to stain isozymes of AChE [8-10]according to the basic principle[11,12]. But in the AFFe method,the $K_4[Fe(CN)_6]$ produced could react with $FeCl_3$ producing the blue deposit Prussian blue ($Fe_4[Fe(CN)_6]_3$), which once was used to stain isozymes of LDH [13], MDH [14]. And the $K_3[Fe(CN)_6$ was also used to stain isozymes of esterase [15] .Once Dithio ethylenediamine was was used to stain isozymes of AChE[16-18],but it is very expensive. Once fast red and naphthylacetate was was used to stain isozymes of AChE [19-20]，but its specificity is not strong.

So the AFCu method to stain the AChE isozymes should be the best one under the existing conditions.

Thank my student Zhaodong Guo for helping to process the words of the paper.

References

[1] D.Ye, B. Chen and Z. He:Journal of Anhui Agricultural Science Vol.39,no.7 (2011),p.3811-3814. (in Chinese)

[2] M. C. Dinamarca，J. P. Sagal，R. A. Quintanilla，J. A. Godoy， M.S. Arrázola and N. C. Inestrosa:Molecular Neurodegeneration Vol.5(2010),p.4-15.

[3] J. J. Nair, A. O. Aremu, J. van Staden:Journal of Ethnopharmacology Vol.137(2011), p.1102–1106.

[4] Z. Yang， J. Ren， P. Xue， M. Yang:Chinese Journal of Experimental Traditional Medical Formulae Vol.17,no.6(2011),p.194-196. (in Chinese)
[5] Y. Ding , S. Yan , R. Xie and B. Huang:Chinese Journal of Tropical Agriculture Vol．31, no.6(2011),p.21-23. (in Chinese)
[6] G. M. Chuiko:Comparative Biochemistry and Physiology Part C Vol．127, no．3(2000),p. 233-242.
[7] Y. Zhao:*Theory and Practice of Biochemical Techniques*. (Wuhan University Press, Wuhan in China 1994). p.287-321. (in Chinese)
[8] H. Zhang, Z.Xing and M.Sun:Military Medical Sciences，no.6(1983),p.689-692. (in Chinese)
[9] S. Qu, S. He, Y. Huangfu, P. Jiang and S. Luo:Chinese Journal of Biochemistry and Molecular Biology Vol.1,no.4(1985),p.29-35. (in Chinese)
[10] S. Li and D. Fan:China Environmental Science Vol.17,no.2(1997),p.163-165. (in Chinese)
[11] M. J. Karnovsky and L. Roots:Journal of Histochemistry and Cytochemistry Vol.12(1964), p.219-221.
[12] A. EL-Badawi and E. A.Schenk:The Journal of Histochemical and Cytochemistry Vol.15, no.10(1967),p.580-588.
[13] G. Zhao , S. Zhang,X. Huang,F. Zhan and A. He:Progress in Biochemistry and Biophysics Vol.27,no.4(2000),p.438-439. (in Chinese)
[14] G. Zhao , S. Zhang, W. Lin, H. Huang, F. Zhan and A. He:Acta Agriculturae Universitatis Jiangxiensi Vol.22,no.4(2000),p.589-590. (in Chinese)
[15] G. Zhao,F. Qian, B. Ling and Y. Cao:Journal of Shanghai Jiaotong University (Agricultural Science) Vol.21,no.Suppl. (2003),p.87-90. (in Chinese)
[16] P. Juul:Clinica Chimica Acta Vol.19,no.2(1968),p.205-213.
[17] D. Wang，S. Wang, C. Li and X. Wang: Railway Occupational Safety Health and Environmental Protection, no.4(1983),p.62-65. (in Chinese)
[18] D. Chen; D. Shen:Journal of Chongqing Medical University Vol.12,no.4(1987),p.230-234. (in Chinese)
[19] D.Yao, R. Ni, J. Huang and X. Meng:Medical Journal of Communications Vol.5, no.1(1991), p.53-55. (in Chinese)
[20] Y. Liu, Y. Li , T. Fu and Q. Zhang: Progress in Veterinary Medicine Vol.26,no.7(2005),p.53-56. (in Chinese)

Advanced Materials Research Vols. 641-642 (2013) pp 7-10

doi:10.4028/www.scientific.net/AMR.641-642.7

Synthesis of 1,1-Bis(hydroxymethyl)cyclopropane as Intermediate for Montelukast Sodium

LI Shu'an[1,a], LI Runlai[2], ZHANG Zhenming[1], YE Sheng[1], WANG Guocheng[1], LIU Hanghang[1]

[1]Jiangsu Research and Development Institute of Marine Resources, Huaihai Institute of Technology, Lianyungang 222005

[2] Department of Chemical and Biomolecular Engineering, Hong Kong University of Science and Technology, Hong Kong

[a]li_shuan@yahoo.com.cn

Key words: Montelukast Sodium, Intermediate, 1,1-Bis(hydroxymethyl)cyclopropane, Synthesis

Abstract. 1,1-Bis(hydroxymethyl)cyclopropane was synthesized by reaction dibromoneopentyl glycol with zinc powder at mole ratio of n_{DG}:n_{zinc}=1:1.05 and 80^{o}C (slightly reflux) for 7 hours. Under optimal conditions, yield and purity of the title compound were 87.3% and 98.67%, respectively. Dibromoneopentyl glycol was also prepared in 91.7% yield with pentaerythritol and hydrobromic acid as material and diethyl sulfate as catalyst under reflux for 10 hours. Structural characterization of 1,1-bis(hydroxymethyl)cyclopropane was conducted by IR and H-NMR.

Introduction

1,1-Bis(hydroxymethyl)cyclopropane is an essential intermediate for synthesis montelukast sodium, developed by Merck and came into market in Finland and Mexico in February 1998. Montelukast sodium is an effective and safe medicine for asthma and allergies of low toxicity.

At present, the reports on synthesis of 1,1- bis(hydroxymethyl)cyclopropane are rare. The three synthesis methods had been reported as follows: (1) firstly1,1-cyclopropanedicarboxylate ester was prepared by the reaction of selenone and malonic ester in alkaline medium, then reduced with LiAlH4 to give title compound. This method involves multi steps synthesis and hence total yield is low. Furthermore, the organic compounds containing selenium can cause damage to human body when exceed dose was ingested. (2) Diethyl 1,1-cyclopropanedicarboxylate is prepared from the reaction of diethyl malonate and 1,2-dichloroethane (or 1,2-dibromoethane) in the presence of phase transfer catalyst, then reduced by metal hydride in the presence of catalyst of aluminum chloride to yield 1,1-bis(hydroxymethyl)cyclopropane. This method requires a large amount of catalyst and reagents, which will be quite cost and a lot of aluminum chloride effluent will be discharged. (3) 1,1-bis(hydroxymethyl)cyclopropane can be obtained by lithium hydride reduction of with halogenated alkylidenemalonate, which prepared by reaction alpha halogenated aldehyde and malonic ester catalyzed with weak base. The materials and catalyst involved the reactions are all expensive.

The reaction between dibromoneopentyl glycol and zinc in ethanol was studied to prepared 1,1-bis(hydroxymethyl)cyclopropane in this paper. Meanwhile, using dimethyl sulfate as catalyst, reaction of pentaerythritol and hydrobromic acid was investigated under reflux reaction to give dibromoneopentyl glycol. The reaction equation is shown as Scheme 1.

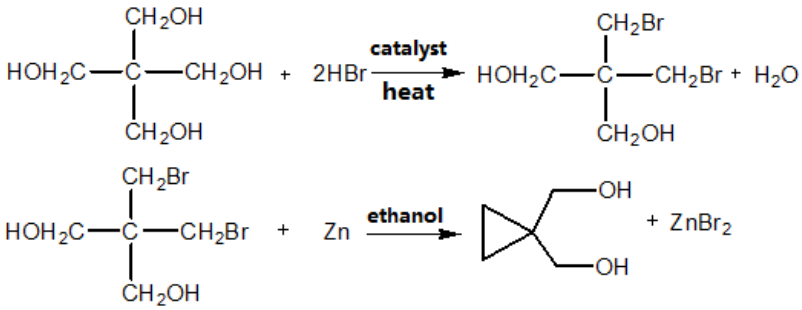

Scheme.1 Reaction formula for synthesis 1,1-Bis(hydroxymethyl)cyclopropane

Experiment

Reagents and Equipment

Reagents: pentaerythritol, hydrobromic acid (40%), dimethyl sulfate, concentrated sulfuric acid, glacial acetic acid, dibromoneopentyl glycol, zinc powder and distilled water.

Equipment and instruments: SGWX-4 melting point detector; PE2400-1 elemental analyzer (PE, U.S.); LC-10ADVP liquid chromatograph (Shimadzu, Japan); chromatographic column C18 (4.6 mm×250 mm, 5μm), mobile phase is methanol-water solution (70:30), flow rate 1mL/min, temperature of column is 45°C, detect wavelength is 235 nm, retention time of 1,1-bis(hydroxymethyl)cyclopropane is 0.5 min. Bruker-VECTOR22 FT-IR (KBr tablet). Bruker AVANCE AV 400 NMR (D_2O as solvent, and TMS as interior standard).

Synthesis of Dibromoneopentyl Glycol

With stirring, 20 g (0.146 mol) pentaerythritol, 68 g (0.40 mol) 47% HBr and 16.6 g (0.108 mol) $(C_2H_5)_2SO_4$ was added in order to a four neck flask equipped with electrical stirring, water separator (linked with condensation reflux pipe) and thermometer, and refluxed for 2 hours at 115°C. Added 3.2 g (0.054 mol) glacial acetic acid then refluxed for another 8 hours. Reactant was distilled under reduced pressure to give sticky solid with light orange. By-product was removed by wash with ethanol-water solution (volume ratio=20:1). After recrystallization, 35.4 g white crystalline solid was obtained with yield of 91.7% and mp 112-113°C (literature: 109 °C). Theoretical value of elemental analysis based on $C_5H_{12}O_4$ (%):C 22.93, H 3.85, observed value (%): C 22.90, H 3.82. IR(cm^{-1}, KBr): 3298 (s), 2952 (m), 1460 (w), 1056 (s).

Synthesis of 1,1-Bis(hydroxymethyl)cyclopropane

20 g (0.076 mol) dibromoneopentyl glycol, 64 mL (1.044 mol) 95% ethanol and 32 mL (1.78 mol)distilled water were fed to a three neck flask equipped with mechanical stirring, condenser with bulb tube and thermometer, then started stirring and added 5.2 g (0.080 mol) Zinc powder slowly. Keep reaction with stirring at refluxed temperature for 7 hours. Removed ethanol by distillation and filtrated to obtain zinc bromide solid. Added activated carbon in the filtrate to adsorb impurities and pigment, then a transparent colorless solution obtained. A light yellow 1,1-bis (hydroxymethyl) cyclopropane (6.8 g) could be collected with yield of 87.3% and purity 98.67% after distillation under reduced pressure to remove ethanol and water. Theoretical value of elemental analysis based on $C_5H_{12}O_2$ (%):C 58.80,H 9.87, measured value(%):C 58.61,H 9.82;IR(cm^{-1},KBr)：3478(s), 2980(m), 1456(w), 1038(s). H-NMR(400MHz, D_2O, $\times10^{-6}$) δ: 4.686(2H, s, H_e, H_f), 3.384(4H, s, H_c, H_d), 0.385(4H, s, H_a, H_b).

Results and Discussion

(1) Effect of feed molar ratio on yield of 1,1-Bis(hydroxymethyl)cyclopropane

If feed molar ratio is no proper, apart from generating target product there can be half condensation or cycilzation of two molecules, which will decrease quantity of target product. Kept dosage of dibromoneopentyl glycol and solvent, reaction temperature and time, procedure and method unchanged, altering addition of zinc powder to investigate effect of feed molar ratio on yield of 1,1-bis(hydroxymethyl)cyclopropane, as shown in Tab.1.

Tab. 1 Effect of molar ratio of dibromoneopentyl glycol to zinc powder on yield of 1,1-Bis(hydroxymethyl)cyclopropane

No.	dibromoneopentyl glycol (mol)	Zinc powder(mol)	$n_{\text{dibromoneopentyl glycol}}:n_{\text{Zinc}}$ (mol/mol)	yield(%)
1	0.076	0.072	1:0.95	65.6
2	0.076	0.074	1:0.97	74.0
3	0.076	0.076	1:1	81.7
4	0.076	0.080	1:1.05	87.3
5	0.076	0.088	1:1.16	87.7
6	0.076	0.092	1:1.21	87.9

Stoichiometric proportion of dibromoneopentyl glycol and zinc powder was 1:1, it could be observed that the yield was only 85.7% when feed molar ratio was 1:1 and 87.3% when feed molar ratio was 1:1.05. But there was not obvious increase of yield if continue increasing addition of zinc powder. Thus it could be determined that the optimum feed molar ratio of synthesizing 1,1-bis(hydroxymethyl)cyclopropane with dibromoneopentyl glycol and zinc powder was 1:1.05.

(2) Effect of reaction temperature on yield of 1,1-Bis(hydroxymethyl)cyclopropane

Ethanol and water were used as solvent in this reaction, kept dosage of material and solvent, reaction time, procedure and method unchanged as experiment 1.3, altering reaction temperature to be 50^{o}C,60^{o}C,70^{o}C and 80^{o}C respectively to investigate effect of reaction temperature on yield of 1,1-bis(hydroxymethyl)cyclopropane, as shown in Tab.2.

Tab.2 Effect of reaction temperature on yield of 1,1-Bis(hydroxymethyl)cyclopropane

No.	Reaction Temperature(^{O}C)	Yield (%)
1	50	20.1
2	60	48.3
3	70	69.2
4	80	87.3
5	85	85.8

It could be observed from Tab.2 that yields of product increased as temperature increased. When it was 80^{o}C reaction solution refluxed gently with the yield of 87.3%. When reflux got faster, yield decreased possibly due to evaporation of some ethanol which made the temperature reach 85^{o}C and by-product (1,1,4,4-tetrakismethylcyclohexane) increase. Thus it could be determined that the optimum reaction temperature be 80^{o}C.

(3) Effect of reaction time on yield of 1,1-Bis(hydroxymethyl)cyclopropane

In the reaction zinc powder was slightly overdose, and the reaction time mainly depended on remaining quantity of zinc powder, as shown in Tab.3.

Tab.3 Effect of reaction time on yield of 1,1-Bis(hydroxymethyl)cyclopropane

No.	Reaction Time(h)	Yield (%)
1	5	68.4
2	6	83.6
3	7	87.3
4	8	86.6

It could be observed in Tab.3 that yield increased as reaction time increased and it reached 87.3% when reacted for 7 hours. Yield would decrease if reacted for more time due to generation of crystalline by-product. Thus it could be determined that the optimum reaction time should be 7 hours.

Conclusions

1,1-Bis(hydroxymethyl)cyclopropane was synthesized by reaction dibromoneopentyl glycol with zinc powder at mole ratio of n_{DG}:n_{zinc}=1:1.05 and 80^{o}C (slightly reflux) for 7 hours. Under optimum conditions, yield and purity of the title compound were 87.3% and 98.67%, respectively. Dibromoneopentyl glycol was also prepared in 91.7% yield with pentaerythritol and hydrobromic acid as material and diethyl sulfate as catalyst under reflux for 10 hours.

Reference:

[1] Li J-J, Modern Pharmaceutical Synthesis, 2005:210-211.

[2] Chen Y., Yang J. Illustration on Synthesis Route of Montelukast Sodium, Journal of China Medicine, 2009,40(1):64-66.

[3] Chen Q., He M.J., Liu J.M., progress of study on relationship between leukotrienes and athma, Journal of pediatrics medicine, 2008,23(16):1284-1286.

[4] Sampson A,Holgate S, Leukotrience modifiers in the treatment of asthma, British Medical Journal,1998,316(5):1257—1258.

[5] Bai G.F., Observation on Treatment of Montelukast Sodium for bronchial asthma of the elder[J], Guidance of China Medicine, 2010, 8(8):76-78.

[6] Ying H.X., Observation on Treatment of Montelukast Sodium for serious bronchial asthma of Children[J], Journal of China General Medicine, 2009, 12(3): 245-246.

[7] Bagnoli L, Scarponi C, Testaferri L, et al. Preparation of both enantiomers of cyclopropane derivatives from the reaction of vinyl selenones with di-(-)-bornyl malonate[J].Tetrahedron: Asymmetry 20 (2009) 1506-1514.

[8] Yao X.F., Progress on Study Effect of Se on human health [J].Silicon Valley,2008,(18):17-18.

[9] Itoh O, Kohmura Y, Ichikawa Y et al. The chemistry of 1,3-glycol derivatives.III.The Preparation of 1,1-Bis(1-hydroxyalkyl)cyclopropanes and Their Halogenation[J]. Bulletin of the Chemical Society of Japen, 1980, 53(1):146-153.

[10] Verhe R, Courtheyn D, Kimpe N D et al. Synthesis of 1,1-bis (hydroxymethyl) cyclopropanes[J]. Organic Preparations and Procedures International: The New Journal for Organic Synthesis, 1981, 13(1): 13-18.

[11] Cao F.C., Synthesis and Application of reactive Fire Retardant of 2,2-bis(bromomethyl)-1,3-propanediol [J].Chemical Engineering of Hebei,1997,(2)19-20.

Advanced Materials Research Vols. 641-642 (2013) pp 11-17

doi:10.4028/www.scientific.net/AMR.641-642.11

The Photocatalytic Properties of Br-doped Titania Nanotube Arrays and its Application in Degradation of Sugar Wastewater

Zhipeng Meng[1,a], Fuxin Zhong[2,b], Danyu Wang[3,c], Zhongming Zhang[4,d], Huaying Li [5,e], Fengjiao Li[6,f]

[1]College of Chemistry and Bioengineering, Guilin University of Technology, Guilin 541004, China,

[2]College of Chemistry and Bioengineering, Guilin University of Technology, Guilin 541004, China,

[3]College of Chemistry and Bioengineering, Guilin University of Technology, Guilin 541004, China,

[4]College of Chemistry and Bioengineering, Guilin University of Technology, Guilin 541004, China,

[5]College of Chemistry and Bioengineering, Guilin University of Technology, Guilin 541004, China,

[6]College of Chemistry and Bioengineering, Guilin University of Technology, Guilin 541004, China

[a]email:gllgmzp@163.com, [b]email:18978368489@189.cn, [c]email:491471817@qq.com,

[d]email:609647774@qq.com, [e]email:375907659@qq.com, [f]email:766707379@qq.com

Keywords: Titania dioxide nanotube arrays, Methyl orange, Photocatalytic degradation, Sugar wastewater

Abstract: This paper presents a novel approach for preparing titanium dioxide nanotube arrays (TNTs) loaded with highly dispersed Br through an ultrasound aided photochemical route. The content of Br doped on the arrays was controlled by changing the concentration of NaBr and the ultrasound time. The Br doped TiO_2 nanotube arrays were characterized by SEM, XRD and UV–Vis spectrum. Doping the bromine did not basically affect the morphology of the surface of the TNTs, but part of the anatase phase transformed into rutile phase, which led to the formation of the mixed crystal and increased the photocatalytic activity. The results showed that Br doping significantly enhanced the photocatalytic degradation rate of titanium dioxide nanotube arrays under UV-light irradiation. The main factors which affected photocatalytic degradation of sugar wastewater were the illumination time and pH. The results showed that the longer the exposure time was, the initial pH of wastewater was more favorable to photocatalytic degradation of the sugar wastewater for the Br-TiO_2 nanotube arrays, and compared to undoped TiO_2 nanotube arrays Br doped TiO_2 nanotube arrays had better photocatalytic properties.

1. Introduction

Titanium dioxide is an important inorganic heterogeneous photocatalytic material, which mainly includes three kinds of morphology, such as abrookite, anatase and rutile. Due to the characteristics of the high photocatalytic activity, chemical stability, abrasion resistance of titanium dioxide, and also the absorption and utilization of partial sunlight, sources adequate and non-toxic, etc., in the solar energy storage and utilization, electro-optical conversion, photochromic and photocatalytic degradation of pollutants in the atmosphere and water have broad application prospects, and become one of the key study subjects.[1,2,3,4,5] TiO_2 becomes one of the key research topics. Since titanium dioxide is a wide band gap semiconductor, it can only absorb UV light whose wavelength is shorter than 387nm. However, as the absorption spectrum only makes up of a small part of the solar spectrum, it is not able to take full advantage of solar. Many of the previous study found that the charge carried generated by the titanium dioxide which was excited by the light exciton were easy to compound, thereby, improving the quantum efficiency of titanium dioxide also became one of the focus of the study. In order to overcome these shortcomings, people have done a

lot of exploration and research, obtained certain achievements, finding that doped titanium dioxide was the most effective method. In this paper, the titanium dioxide nanotube arrays (TNTs) were prepared by the anodic oxidation method, while Br-TNTs were prepared by ultrasonic immersion method. We not only studied the performance of the photocatalytic degradation of methyl orange, but also explored its application in the photocatalytic degradation of sugar wastewater, so as to achieve the objective which makes sugar wastewater containing high concentration of organic compounds eventually degraded to H_2O, CO_2 and other inorganic small molecule.

2. Experiment

2.1Main instruments and reagents

2.1.1Instruments

WWL—LDX precision linear stabilized DC regulated power supply, TCW-32B box furnace, UV-2450 ultraviolet-visible spectrophotometer, SK2210LHC ultrasonic cleaner, GSM-6380LV scanning electron microscopy, X´Per Pro X-ray diffract meter, CJJ78-1 heat-up magnetic agitator.

2.1.2 Reagents

Ethanol(AR), Hydrofluoric acid(AR), Nitric acid(AR), Sodium bromide(AR), Methyl Orange(AR), Hydrochloric acid(AR), NaOH(AR),Industrial pure titanium plate.

2.2 Sample preparation

The industrial pure titanium plate was cut into 4.5cm×1cm. In order to get rid of the oil impurities of the surface, under the ultrasonic condition, the titanium plates were respectively cleaned by ethanol and deionized water for 10min. Next, titanium plates were rapidly dried by a blower. The titanium plate was mechanically and chemically polished to a high mirror finish in a mixture of HF: HNO_3 with 1:1 in volume, followed by rinsing thoroughly with deionized water. A two-electrode electrochemical cell consisting of the titanium plate and Pt counter electrode under 20V for 20 min were previously described in the literature[6].The prepared samples were annealed in a box furnace (TCW-32B, Shanghai, China) at 500°C for 2 h. Finally, the sample was immersed in NaBr aqueous solution for 20min with an ultrasonic generator (KQ100DB, Kun shan Ultrasonic Instrument Co., Ltd., China).

2.3 Performance testing

Using 20W lamp(λ=253.7nm) as a light source, the sample distanced from the light source 12cm.The preparation conditions and photocatalytic activities of the samples were evaluated by the degradation of Methyl Orange at room temperature. Sugar wastewater which was diluted took the place of the methyl Orange, changing UV irradiation time and the pH of the solution of the sugar wastewater, which investigated the conditions of photocatalytic degradation of sugar wastewater on the Br-TNTs. The absorbance values of Methyl Orange were measured at a wavelength of 463nm before and after the illumination. What's more, the absorbance values of sugar wastewater were measured at a wavelength of 299nm.The photocatalytic activity was evaluated by the degradation rate. The degradation rate (M) was calculated by the following formula:

$M = (A_0 - A) / A_0 \times 100\%$, where A_0 and A are absorbance of initial and the instant during the reaction respectively.

2.4 The characterization methods of TNTs and Br-TNTs

The surface morphology and crystal phase of TNTs and Br-TNTs were analyzed by using scanning electron microscopy (SEM) and X-ray diffraction (XRD).

3. Results and discuss

3.1 The structural characterization of TNTs and Br-TNTs

3.1.1 Analysis of the sample morphology

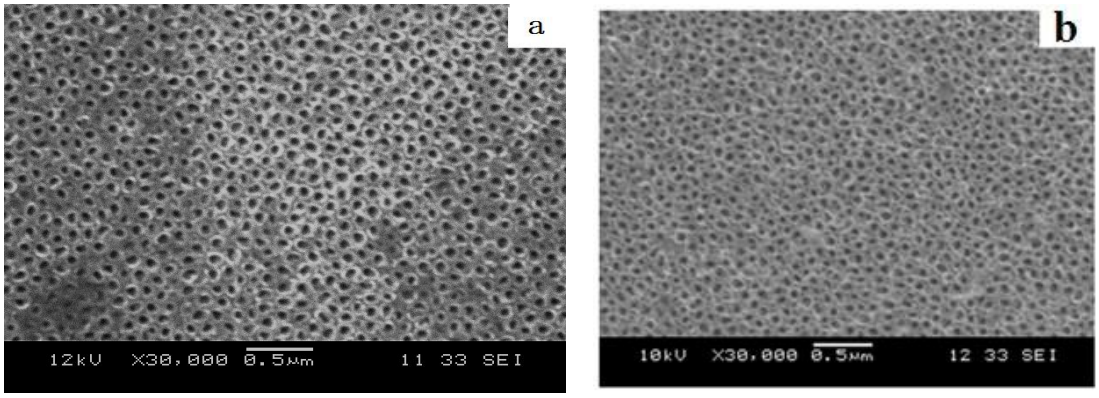

Fig.1 SEM micrographs of the bromine-doped titania nanotube arrays(a) and non-doped titania nanotube arrays(b)

Fig.1 (a) and (b) show the SEM image of Br doped TiO_2 nanotube arrays and TiO_2 nanotube arrays respectively. In the figure, the morphology of the doped and undoped nanotubes has great similarity. Their diameter is more uniform. The array structure is also array in a more regular way. We can also find that the ultrasonic impregnation doping does not cause to much change the structure of the TiO_2 nanotube arrays.

3.1.2 The analysis of XRD

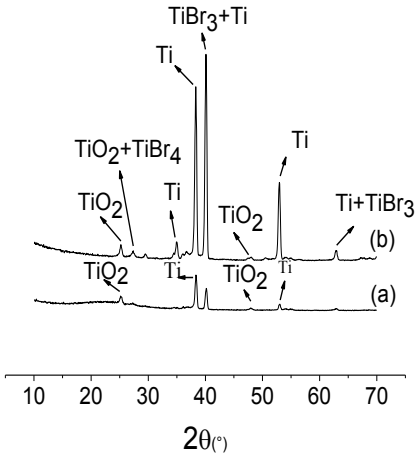

Fig.2 XRD spectra of TNTs（a）and Br-TNTs(b)

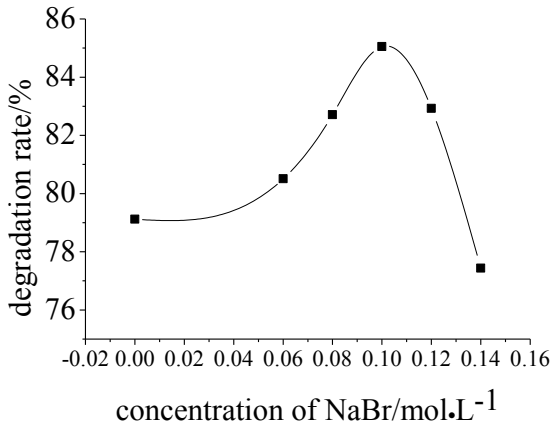

Fig.3 Influence of the concentration of sodium bromine on degradation of methyl orange over Br-TNTs

Fig.2. shows the XRD spectra of TiO_2 nanotube arrays (Fig. 2a) and Br-doped TiO_2 nanotube arrays (Fig.2b). Fig.2(b) shows the samples of the bromine-doped TiO_2 nanotube arrays appeares the characteristic peak of $TiBr_4$ at 2θ=27.34°（222）, and the characteristic peak of $TiBr_3$ appeares at 2θ=40.2° and 2θ=62.93°,which shows that bromine has been doped in the TiO_2 nanotube arrays. In addition, the sample(b) appears the rutile phase of titanium dioxide at about 2θ=27.34°（222）, which shows that the incorporation of bromine makes the part of the anatase phase of titanium dioxide transformed for the rutile phase.

3.2. The determination of the optimal preparation conditions on the Br-TiO_2

3.2.1. The determination of the amount of sodium bromine

Fig.3 shows the Influence of concentration NaBr on the degradation rate of Methyl Orange. The photocatalytic degradation rate increases with the increment of the concentration of NaBr in the initial, but when the concentration of NaBr exceeds 0.01 mol·L^{-1}, the photocatalytic degradation rate shows a downward trend.

3.2.2. The determination of the test ultrasound doping time

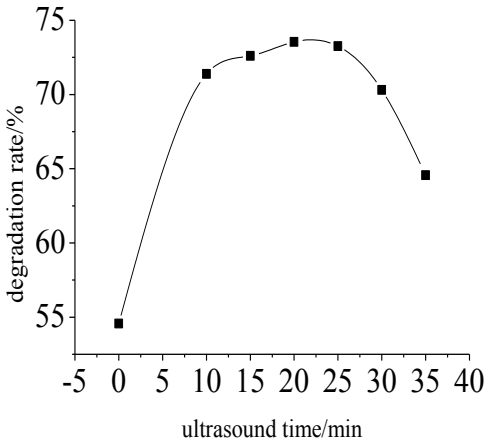

Fig.4 The influence of the ultrasonic time on degradation of methyl orange over Br-TNTs

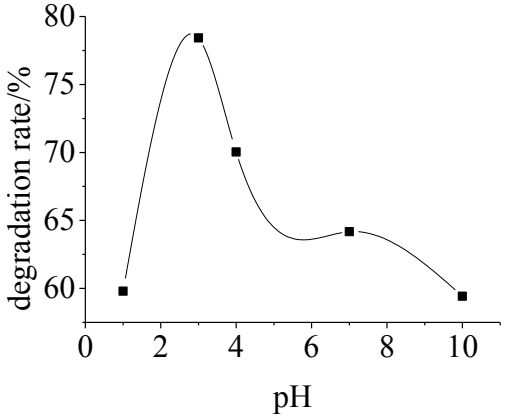

Fig.5 The influence of pH on methyl orange degradation rate

Fig.4 shows the influence of ultrasonic time on the degradation rate of Methyl Orange over Br-TNTs. The photocatalytic degradation rate increases with the increment of the ultrasonic time in the initial, but when the ultrasonic time preponderates over 20 min, the photocatalytic degradation rate begins to show a downward trend.

3.3. Performance Evaluation

3.3.1 Influence of pH

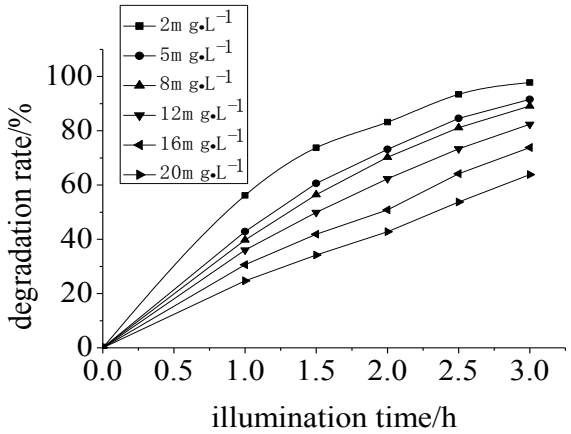

Fig.6 The influence of the the concentration of methyl orange on degradation rate

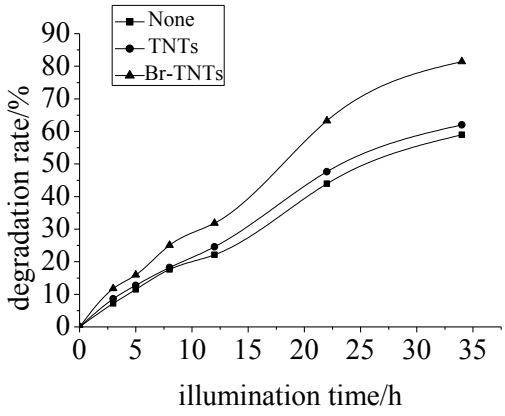

Fig.7 The affect of the illumination time on photocatalytic degradation Sugar wastewater

Fig.5 shows the influence of pH on the degradation rate of methyl orange. When pH value is under 3, the photocatalytic degradation rate increases with the increment of pH, but when the pH is greater than 3, the photocatalytic degradation rate begins to show a downward trend. This may have

a certain relationship with the structure of the methyl orange. Under acidic conditions, methyl orange is the structure of the quinoid. However, under neutral or weak alkaline, it is aze structure. Quinone-type structure breaks down easily under acidic conditions[7]. Furthermore, the smaller the pH value is, the more hydrogen ion can be absorbed on the surface of the TiO_2.This makes the surface of the titania dioxide with positive charge, and contributes to the migration of the photoinduced electrons and oxygen which is absorbed on the titanium dioxide surface react with photoinduced electrons to form peroxy radicals. As a strong oxidant, peroxy radicals contribute to oxidative decomposition of Methyl Orange[8].

3.3.2 Influence of initial concentration

Fig.6 shows the influence of the the concentration of methyl orange on degradation rate. With the same illumination time, the photocatalytic degradation rate decreases with the increment of the initial concentration of Methyl Orange. The possible reason is that the color will deepen with the increase of concentration, which makes the penetration of light weaken to a certain extent in the solution. Furthermore, Titanium dioxide can absorb certain organic compounds, the amount of organic matter contained in the solution increases with the increase of concentrations of the solution, the amount of organic matter absorbed onto the surface of the catalyst also will correspondingly increase, making hydroxide ions which can reach the surface of the titania nanotube relatively reduced, hydroxyl free radical, thereby, compared with the low concentration of methyl orange solution, the photocatalytic degradation rate of the high initial concentration methyl orange also naturally reduces.

3.3.3 Study on the stability of sample

In order to investigate the stability of the catalyst, the same sample of titanium plate is used repeatedly for times. After the same concentration of methyl orange solution is irradiated for 4 h under the 20W ultraviolet lamp(λ=253.7 nm), the photodegraded rate of methyl orange changed little. The result shows that the synthetic bromine-doped TiO_2 nanotube arrays are stable and can be repeatedly used.

3.3.4 The influence of the illumination on photocatalytic degradation of sugar wastewater

Fig.7 shows the effect of the illumination time on photocatalytic degradation sugar wastewater. We can get a best result from the effect of photocatalytic degradation sugar wastewater over bromine doped titanium dioxide. The super photocatalytic activity of bromine-doped titanium dioxide attributed to the modification of bromine.

3.3.5 The influence of pH on photocatalytic degradation of sugar wastewater

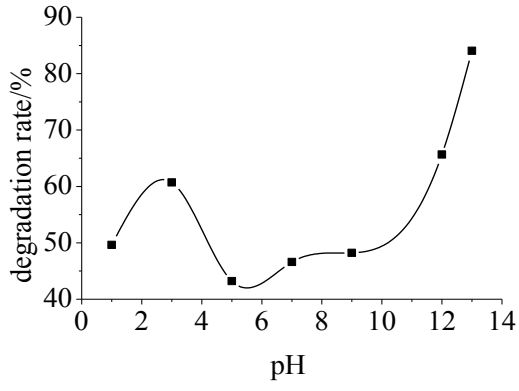

Fig.8 The effect of the pH on photocatalytic degradation of sugar wastewater over Br-TNTs

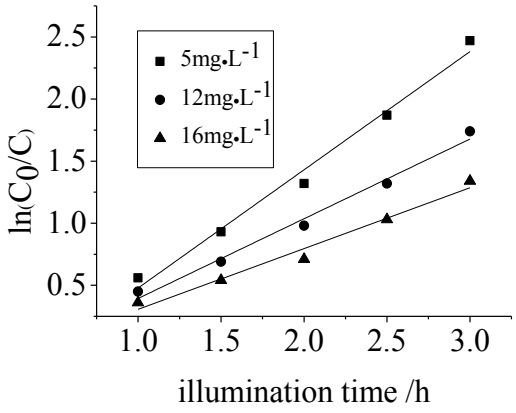

Fig. 9 Relationship of $\ln(C_0/C)$ and t under different concentration of methyl orange

Fig.8 shows the effect of the pH on photocatalytic degradation of sugar wastewater over Br-TNTs. The photocatalytic degradation rate increases noticeably after pH=6, but the photocatalytic degradation rate which first increases and then declines, existing an optimum value. Analysis of the causes: Related research results[9] show that the hydroxyl free radical which is the oxide particles in the photocatalytic oxidation reaction has strong oxidation ability. When the pH is lower, the hydroxyl free radical is mainly formed by the reaction of oxygen absorbed on the surface of the TiO_2 and captured the proton. However, when the pH becomes higher, the hydroxyl free radical is mainly formed by the reaction of hydroxide ions absorbed on the surface of the TiO_2 and trapped photogenerated holes. In this experiment, the strong alkaline conditions are more conductive to the photocatalytic degradation of sugar wastewater.

3.4 Kinetic analysis of the methyl orange degradation

Generally, the photocatalytic decolorization reaction of the methyl orange aqueous solutions follows the Langmuir-Hinshelwood model[10,11,12]:

$$r = -\frac{dC}{dt} = -\frac{k_a K C_0}{1+KC_0} \quad (1)$$

k_a, K and C_0 respectively denote reaction rate constant, adsorption constant and initial concentration of the methyl orange. If the Br-TiO_2 photocatalytic degradation of methyl orange is pseudo first order reaction, the equation can be simplified to an apparent first order equation: $r=k_bC_0$, Further transformation is able to obtain: $\ln(C_0/C)=k_b t$

Where C is the concentration measured at the interval of time, and k_b *is* the apparent first-order rate constant which can be used to evaluate the photocatalytic activity, the values of k_b for pseudo-first-order kinetics of methyl orange photocatalytic decolorization with Br-TiO_2 are listed in Table 1.

Table 1 The first-order reaction kinetics equation of the different concentration of methyl orange

initial concentration C [mg·L^{-1}]	First order equation	Apparent rate constant k_b [h^{-1}]	Correlation coefficient R^2
5	$\ln(C_0/C)$= 0.952t -0.474	0.952	0.98347
12	$\ln(C_0/C)$= 0.353t-0.248	0.642	0.9845
16	$\ln(C_0/C)$= 0.49t -0.184	0.49	0.97074

The kinetic equation and related parameters of the different initial concentrations of methyl orange solution are obtained by the least squares linear fit, listed in Table 1. From the figure 9 and Table1, we can see that the linear relationship of $\ln(C_0/C)$ and the illumination time is better, the correlation coefficient is relatively large, which shows that the degradation rate of methyl orange and the initial concentration of the reactants are associated. The photocatalytic reaction is pseudo first order reaction and conforms to the mechanism of Langmuir-Hinshelwood.

From Table 1, we can see that the apparent rate constant (k_b) decreases with the increase of the initial concentration of methyl orange. the lower initial concentration of methyl orange, the higher the transmittance of the solution, the probability of the photocatalytic degradation of the methyl orange molecules will become larger, the effective utilization of the active groups were improved, and the catalytic efficiency was also enhanced.

4. Conclusions

In summary, we have demonstrated that bromine modified TiO_2 nanotube arrays exhibit high photocatalytic activites in the decolorization of methyl orange aqueous solutions under ultraviolet light irradiation. The photocatalytic degradation of the methyl orange molecules was affected by the doped amount of NaBr, pH, initial concentration of methyl orange and so on. pH and illumination time affected the photocatalytic degradation of sugar wastewater . The pH 13 was proved to be the best conditions for maximum photocatalytic degradation sugar wastewater.

Acknowledgments

This work was partly supported by the Natural Science Foundation of China (Grant No. 61264007).

References

[1] X. H. Li, X. G. Zhang, H. L. Li, Template Synthesis and Characterization of TiO_2 Nanotubules.Chemical journal of chinese universities, 22(2001) 130–132.

[2] M. R.Hoffmann, S. T. Martin, W. Choi, Environmental application of semi conductor photocatalysis, Chem. Rev. 95(1995) 69.

[3] I. Sopyan, M. Watanabe, S. Murasawa. Efficient TiO_2 powder and film photocatalysts with rutile crystal structure, Chem Lett. (1996) 69–70.

[4] U. Bach, D. Lupo, P. Comte, J. E. Moser, F. Weissortel, J. Salbeck, et al. Solid-state dye-sensitized mesoporous TiO_2 solar cells with high photo-to-electron conversion efficiencies, Nature. 395(1998) 583.

[5] C. R. Martin, Nanomaterials a membrane-based synthetic approach, Science. 266 (1994) 1961–1966.

[6] H. M. Zhu, B. F. Yang, J. Xu, Z. P. Fu, M. W. Wen, et al. Construction of Z-scheme type CdS–Au–TiO_2 hollow nanorod arrays with enhanced photocatalytic activity, Applied Catalysis B: Environmental. 90(2009) 463-469.

[7] H. Y. Xu, G. W. Zhou, Y. Q. Wei, Y. J. Li, Synthesis of Si dopedmesoporousTiO_2 and photocatalytic degradation of methyl orange under visible light, New Chemical Materials. 36 (2008)58～61.

[8] Y. R. Zhang, J. Wan, Y. Q. Ke, A novel approach of preparing TiO_2 films at low temperature and its application in photocatalytic degradation of methyl orange, Journal of Hazardous Materials. 177 (2010) 750–754.

[9] J. A. Byme, B. R. Eggins, N. M. D. Brown, Immobilisation of TiO2 powder for the treatment of polluted water, Catalysis Today. 17(1998)25.

[10] S. Song, F. Y. Hong, Z. Q. He, H. Y. Wang, X. H. Xu, J. M. Chen, Influence of zirconium doping on the activities of zirconium and iodine co-doped titanium dioxide in the decolorization of methyl orange under visible light irradiation, Applied Surface Science. 257 (2011)10101– 10108.

[11] H. C.Yatmaz, A. Akyol, M. Bayramoglu, Kinetics of the photocatalytic decolorization of an Azo reactive dye in aqueous ZnO suspensions, Ind. Eng. Chem. Res.43, (2004)6035–6039.

[12] X. H. Wang, J. G. Li, H. Kamiyama, Y. Moriyoshi, T. Ishigaki, Wavelength-sensitive photocatalytic degradation of methyl orange in aqueous suspension over iron(III)-doped TiO2 nanopowders under UV and visible light irradiation, J. Phys. Chem. B 110.(2006) 6804–6809

Advanced Materials Research Vols. 641-642 (2013) pp 18-21

doi:10.4028/www.scientific.net/AMR.641-642.18

Response of antioxidant system in leaves of *Ginkgo biloba* to elevated CO_2 and/or O_3 and its natural recovery in an urban area

Jiang-Yan Gao, Sheng Xu*, Wei Chen, Xing-Yuan He

Institute of Applied Ecology, Chinese Academy of Sciences, Shenyang China
shengxu703@126.com

Keywords: Antioxidative system, Elevated CO_2, Elevated O_3, *Ginkgo biloba*, Oxidative stress

Abstract. Changes of oxidative stress and antioxidant system were studied in leaves of *Ginkgo biloba* exposed to elevated CO_2 and O_3 fumigation (2006-2008), and released the gases fumigation for the natural recovery in open-top chambers (OTCs) during the growing season in 2009. Elevated CO_2 had no significant effect on hydrogen peroxide (H_2O_2) and malondialdehyde (MDA) contents, and the activities of antioxidant enzymes in leaves of *G. biloba* during the gas fumigation in 2008. Elevated O_3 increased significantly H_2O_2 and MDA contents, especially after 90 days of gas fumigation. The adverse effect or damage of elevated O_3 on trees during the gas fumigation was also alleviated by the released-O_3 exposure during the natural recovery. The antioxidative enzyme including superoxide dismutase (SOD), catalase (CAT) and ascorbate peroxidase (APX) activities showed higher levels under the natural recovery than under the gas fumigation, which may be a helpful response to scavenging reactive oxygen species (ROS). The results also indicated that future alleviating the emissions of CO_2 and O_3 would differentially affect the antioxidant system in plants.

Introduction

Rising concentrations of CO_2 and tropospheric O_3, as a result of increasing industrialized activity [1], alter trees performance in both natural and managed ecosystems. Approximately half of the world's forests are expected to experience increased co-exposure of CO_2 and O_3 by 2100 [2]. As a dangerous toxicant, tropospheric O_3 induces production of other reactive oxygen species (ROS) after diffusing into apoplastic solution. ROS were highly phytotoxic and would lead to oxidative stress and cell membrane lipid peroxidation in trees. Fortunately, trees have developed the antioxidant systems to protect plant cells by controlling the intra-cellar ROS content in the changes of enzyme activities [3]. Enzymatic scavenging system includes superoxide dismutases (SOD) (EC 1.15.1.1), which convert the superoxide radical to hydrogen peroxide (H_2O_2), and the catalase (CAT) (EC 1.11.1.6) and peroxidases (primarily ascorbate peroxidase: APX, EC 1.11.1.11). In non-enzymatic scavenging system, antioxidant compounds such as ascorbic acid (ASA) also play important roles in the removal of toxic oxygen compounds.

Elevated CO_2 may reduce the accumulation of ROS in photosynthesis apparatus for increased ratio of CO_2 to O_2 [4]. Both CO_2-induced stimulation and down-regulation of antioxidant systems have been reported [5]. Elevated O_3 may increase the accumulation of ROS [6], decrease [7] or increase [8] the antioxidative enzyme activities in plant. Many studies on plant antioxidant systems in elevated CO_2 and/or O_3 environment are still inconsistent though the studies on the effects of elevated CO_2 and/or O_3 on plant antioxidant systems have been started since the early 1980s [5]. It is still a controversial topic that whether elevated CO_2 can ameliorate the oxidative stress of elevated O_3 on trees.

As we know, tropospheric O_3 levels are increasing parallel to CO_2 concentrations around urban areas [1], therefore, in the future urban trees will be simultaneously experiencing elevated CO_2 and O_3 levels. *G. biloba* is one of the commonly used street trees for urban greening in Shenyang [5].

We have reported responses of the antioxidative systems of many urban trees, including *G. biloba*, to elevated CO_2 or elevated O_3 concentration [9-10], while very little information is known in the aspect of the antioxidative system of plant released from elevated CO_2 and/or O_3 fumigation inder the natural recovery. Here, we reported the oxidative stress and antioxidative results of *G. biloba* under elevated CO_2 and/or O_3 fumigation and its natural recovery, which will provide insights into physiological mechanisms of plant in response or adaptation to climate change, especially under the background of alleviating the increasing tropospheric CO_2 and O_3 in future.

Materials and methods

The experiment was conducted at Shenyang Arboretum, located in the populated central area of Shenyang city, China. Four-year-old of *G. biloba* seedlings were planted on ground of twelve open top chambers (OTCs) in May 2006. Three OTCs for ambient air (CK), elevated CO_2 (700 ppm), elevated O_3 (80 ppb) and elevated CO_2 + O_3 (700 ppm CO_2 + 80 ppb O_3), respectively. CO_2 was injected into the chambers from cylinders 24 h daily and the concentrations were monitored by CO_2 infrared transducer (SenseAir, Sweden). O_3 was added to the OTCs 9 h daily (08:00–17:00). The concentrations of O_3 were monitored by O_3 analyzer (S-900 Aeroqual, New Zealand). The fumigation periods of the two gases were from June to September each year in 2006–2008, and the recovery period without any gas fumigation was from June to September in 2009. The leaves of *G. biloba* were sampled at 9:00–10:00 a.m after 0, 30, and 90 days of gas fumigation in 2008, and on June 22, July 23, and September 22 during the growing season in 2009.

H_2O_2 content was estimated by forming a titanium-hydro peroxide complex [11]. Leaves (0.5 g) were cut into the ceramic crucible with 5 mL cooled acetone and were ground in an ice bath. The reaction mixture was centrifuged at 10,000 *g* for 10 min. H_2O_2 content was determined using a standard curve. MDA content was determined according to the method of Buege and Aust [12]. ASA content was estimated according to Mukherjee and Choudhuri [13]. SOD activity was determined according to the method of Beyer and Fridovich [14]. CAT activity was determined according to the method of Aebi and Lester [15]. For APX activity assay, a 1-mL reaction mixture containing 50 mM K-phosphate buffer (pH 7.0), 5 mM ASA, 2 mM H_2O_2, 10% glycerol, 1mM EDTA, and 0.04 mL of crude enzyme was used. ASA content was estimated according to Chen and Asada [16]. Chambers corresponding to the same treatment were considered statistical replicates. ANOVA was carried out using the SPSS computer package (SPSS Inc. Chicago, IL, USA) for all sets of data. The values presented are means of all measurements and the significance of the differences of means were evaluated by LSD.

Results and discussion

Both of H_2O_2 and MDA contents in leaves of *G. biloba* during the recovery in 2009 were decreased significantly by the released-CO_2 or O_3 exposure, compared to those during the gas fumigation in 2008 (Fig. 1A-B).

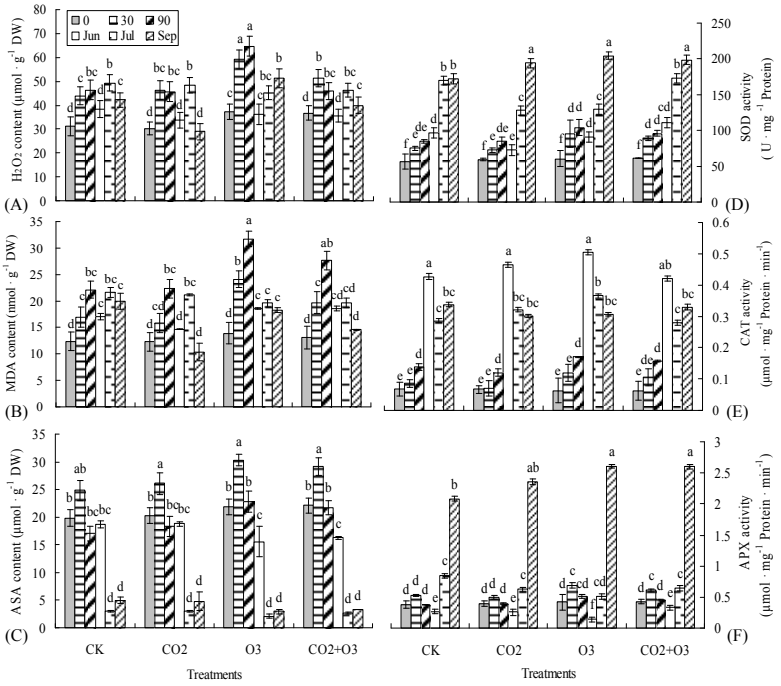

Fig. 1. Changes of hydrogen peroxide (H_2O_2, A), malondialdehyde (MDA, B) and ascorbic acid (ASA, C) contents, superoxide dismutase (SOD, D), catalase (CAT, E) and ascorbate peroxidase (APX, F) activities in leaves of *Ginkgo biloba* fumigated by elevated CO_2 and O_3 during fumigation (after 0, 30 and 90 days of gas fumigation in 2008) and recovery (June 23, July 22 and September 23 in 2009). Data shown are means and standard deviation (SD) of 3–6 replicates. Different lower case letters indicate significant difference at ($P < 0.05$).

Elevated O_3 increased significantly H_2O_2 and MDA contents in 2008 (Fig. 1A-B) ($P < 0.05$). In our study, the combination of elevated O_3 and CO_2 induced lower H_2O_2 and MDA contents than elevated O_3 alone during fumigation in 2008. The adverse effect or damage of elevated O_3 on trees in 2008 was alleviated by the released-O_3 exposure in 2009, implying the enhanced antioxidant level in leaves of *G. biloba* allowed to limit H_2O_2 accumulation under the natural recovery.

ASA plays an important role in antioxidant systems of plants. Our results showed that ASA content in *G. biloba* leaves was maintained at a high level (Fig. 1C). The activities of SOD, CAT and APX in *G. biloba* leaves were increased during natural recovery in 2009 than gas fumigation in 2008 (Fig. 1D-F), which may be a helpful response to scavenging ROS. Elevated O_3 increased the activities of SOD and APX after 30 days of gas fumigation in 2008 (Fig. 1D, 1F). In this study, APX and SOD activities were shown higher level in 2009 than in 2008 for plants exposed to elevated O_3. Similar results were reported by our studies in other tree species [10].

Conclusion

The results showed that elevated CO_2 alleviated oxidative stress of elevated O_3 on *G. biloba*. The adverse effect or damage of elevated O_3 on trees during the gas fumigation was also alleviated by the released-O_3 exposure during the natural recovery. The antioxidative enzyme activities in *G. biloba* leaves showed higher levels under the natural recovery than gas fumigation. These results will provide insights into physiological mechanisms of plant in response to climate change, especially under the background of alleviating the increasing tropospheric CO_2 and O_3 in future.

Acknowledgments

This research was supported by the National Natural Science Foundation of China (31170573, 31270518), and the National Natural Science Key Project (90411019).

References

[1] IPCC. Climate Change, "The physical scientific basis. Contribution of Working Group I to the Fourth Assessment Report of the Intergovernmental Panel on Climate Change (IPCC)," Cambridge University Press, Cambridge, UK, 2007, pp. 996.

[2] B.J. Kopper and R.L. Lindroth, "Responses of trembling aspen (*Populus tremuloides*) phytochemistry and aspen blotch leafminer (*Phyllonorycter tremuloidiella*) performance to elevated levels of atmospheric CO_2 and O_3," Agr. Forest Entomol. 5 (2003) 17-26.

[3] S. Xu, X.Y. He, W. Chen, D.L. Tao, W.D. Xu, (2009) "Impact of elevated O_3 on eco-physiology of trees," Acta Ecol. Sin. 29 (2009) 368-376 (in Chinese).

[4] D.F. Karnosky, "Impacts of elevated atmospheric CO_2 on forest trees and forest ecosystems: knowledge gaps," Environ. Int. 29 (2003) 161-169.

[5] T. Lu, X.Y. He, W. Chen, K. Yan, T.H. Zhao, "Effects of elevated O_3 and/or elevated CO_2 on lipid peroxidation and antioxidant systems in *Ginkgo biloba* leaves," Bull. Environ. Contam. Toxicol., 83 (2009) 92-96.

[6] R. Mahalingam, N. Jambunathan, S.K. Gunjan, E. Faustin, H. Weng, P. Ayoubi, "Analysis of oxidative signaling induced by ozone in *Arabidopsis thaliana*,". Plant Cell Environ. 29 (2006) 1357-1371.

[7] T. Zhao, J. Wang, Y. Wang, Y. Cao, "Effects of antioxidant enzymes of ascorbate-glutathione cycle in soybean (*Glycine max*) leaves exposed to ozone," Adv. Mater. Res. 204-210 (2011) 672-677.

[8] K.M. Gillespie, A. Roger, E.A. Ainsworth, "Growth at elevated ozone or elevated carbon dioxide concentration alters antioxidant capacity and response to acute oxidative stress in soybean (Glycine max)," J. Exp. Bot. 62 (2011) 2667-2678.

[9] Y. Ruan, X. He, W. Chen, Z. Chen, Y. Sun, "Effects of elevated CO_2 concentration on anti-oxidative enzyme activities of urban *Pinus tabulaeformis*," Chin. J. Ecol., 28 (2009) 839-844.

[10] X. Li, X. He, W. Chen, S. Xu, K. Yan, "Effects of elevated O_3 and CO_2 on the antioxidant enzyme activities in *Pinus tabulaeformis* needles," Chin. J. Ecol. 28 (2009) 2220-2226 (in Chinese).

[11] P. Dagmar, R.K. Sairam, G.C. Srivastava, D.V. Singh, "Oxidative stress and antioxidant activity as the basis of senescence in maize leaves," Plant Sci. 161(2001) 765-771.

[12] J.A. Buege and S.D. Aust, "Microsomal lipid peroxidation," Meth. Enzymol. 52 (1978) 302-310.

[13] S.P. Mukherjee and M.A. Choudhuri, "Implications of water stress-induced changes in the levels of endogenous ascorbic acid and hydrogen peroxide in Vigna seedlings," Physiol. Plant 58 (1983) 166-170.

[14] W.F. Beyer and I. Fridovich, "Assaying for superoxide dismutase activity: some large consequences of minor changes in conditions," Anal. Biochem. 161 (1987) 559-566.

[15] H. Aebi and P. Lester, "Catalase in vitro," Meth. Enzymol. 105 (1984) 121-126.

[16] G.X. Chen and K. Asada, "Ascorbate peroxidase in tea leaves: occurrence of two isozymes and the differences in their enzymatic and molecular properties," Plant Cell Physiol. 30 (1989) 987-998.

Advanced Materials Research Vols. 641-642 (2013) pp 22-25

doi:10.4028/www.scientific.net/AMR.641-642.22

Photosynthetic responses of four urban tree species exposed to elevated CO_2 and /or elevated O_3

Sheng Xu, Jiang-Yan Gao, Wei Chen, Xing-Yuan He*, Yan-Qing Huang

Institute of Applied Ecology, Chinese Academy of Sciences, Shenyang China
hexy1962@126.com

Key words: Global climate change, Photosynthesis, Urban tree species

Abstract. We compared the differences in photosynthesis of four urban tree species (*Ginkgo biloba, Pinus tabulaeformis, Quercus mongolica* and *Pinus armandii*) exposed to long-term elevated CO_2 (700 ppm) and/or O_3 (80 ppb) fumigation in (open top chamber) OTC. Our results showed that elevated CO_2 alleviated the damaging influence of elevated O_3 on photosynthesis in the four urban tree species. Both *Q. mongolica* and *P. armandii* showed photosynthetic acclimation after long-term treatment under elevated CO_2. The combined effect of elevated CO_2 and O_3 caused the changes including net photosynthetic rates (Pn), stomatal conductance (gs) and chlorophyll content that were more similar to ambient air (CK) or slightly lower than elevated CO_2, indicating that elevated CO_2 is able to totally or partly alleviate the harmful effects of elevated O_3 on urban tree species.

Introduction

It is predicted that the end of this century, the average level of CO_2 and O_3 in the Earth's atmosphere is going to reach 700 ppm and 80 ppb, respectively [1]. Approximately half of the world's forests are expected to experience increased co-exposure of CO_2 and O_3 by 2100 [2]. In general, elevated CO_2 stimulates tree growth, biomass and leaf area [3]. As a phytotoxic secondary air pollutant, O_3 usually decreases growth, damages photosynthetic apparatus and disturbs the physiological processes of trees [4].

The combined effects of elevated CO_2 and O_3 on photosynthesis of trees have been investigated but the results are often contradictory. As we know, tropospheric O_3 levels are increasing parallel to CO_2 concentrations around urban areas with development of urbanization, therefore, in the future urban trees will be simultaneously experiencing elevated CO_2 and O_3 levels [5]. It is not clear whether elevated CO_2 reduces the detrimental effects of O_3 on photosynthesis of urban trees.

Ginkgo biloba and *Quercus mongolica* are the two economically and ecologically important temperate deciduous tree species in China. *Pinus tabulaeformis* and *Pinus armandii* are the two endemic and dominant species of coniferous forest for timber and soil conservation in China. They also widely are used for landscape ornament and forestation in the urban area of northeast China. In recent years, we have reported physiological responses of these urban trees, especially in the antioxidant systems of these urban trees exposed to elevated CO_2 or elevated O_3 [6-7], while very little information is known for the responses of photosynthesis of the different urban tree species.

Here we compared the differences in photosynthesis of the four urban tree species exposed to elevated CO_2 and/or O_3 concentration, which will provide a scientific reference for the management and sustainable development of urban forest under the background of global climate change.

Materials and methods

The study was conducted at Shenyang Arboretum, located in the populated central area of Shenyang city, China. Four-year-old *G. biloba*, *P. tabulaeformis*, *Q. mongolica* and *P. armandii* were planted on ground (loamy soil, no extra fertilizer) of twelve open top chambers in May 2006. Three OTCs for ambient air (CK), elevated CO_2 (700 ppm), elevated O_3 (80 ppb) and elevated CO_2 + O_3 (700 ppm CO_2 + 80 ppb O_3), respectively. The trees were randomly distributed among the chambers. The concentrations of CO_2 and O_3 in OTCs were controlled by a computer. Complete details on the experimental design and gases generation and monitoring can be found in our recent studies [7]. The gases fumigation periods were from 2006 to 2008 during growth season. All the data in this study were obtained on June 18, July 20, August 20 and September 22 in 2008.

Gas exchange measurements were measured by a photosynthesis system (LI-6400, USA). Chlorophyll content was measured in leaves or needles extracts with 100% acetone. One-way analysis of variance (ANOVA) was performed using SPSS computer package (10.0 SPSS, USA) for all sets of data, and the significance of differences between treatments were estimated by LSD. Sample variability is given as the standard deviation (SD) for presentation.

Results and discussion

Many studies have shown that elevated CO_2 lead to increased net photosynthetic rate (Pn) of plants. In our studies, elevated CO_2 increased Pn of every urban tree species at the beginning of growing season (Fig. 1). However, no significant increase in Pn of *G. biloba* and *P. tabulaeformis* or even slight decrease in *Q. mongolica* and *P. armandii* under elevated CO_2 (Fig. 1).

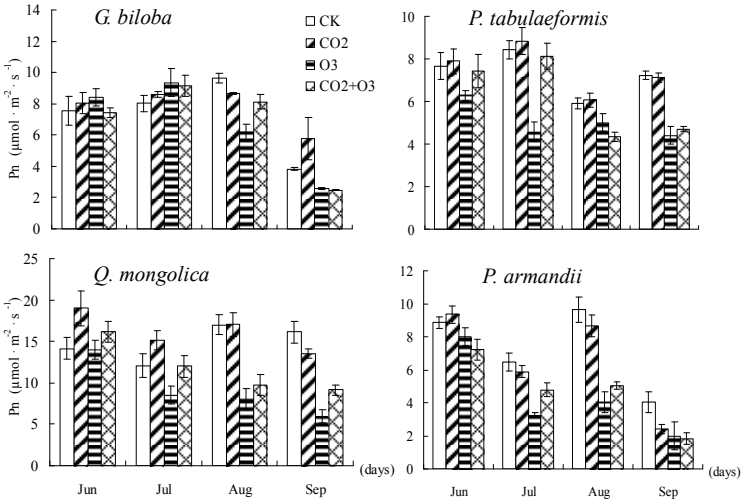

Fig. 1. Effects of elevated CO_2 and/or O_3 on net photosynthetic rates (Pn) in leaves of *G. biloba* and *Q. mongolica*, and previous-year needles of *P. tabulaeformis* and *P. armandii* in 2008. Data are means ± SE (n=9).

As we know, the CO_2-induced stimulation of photosynthesis has often been found to decrease (down-regulation) under long-term CO_2 exposure [8]. We inferred that *Q. mongolica* and *P. armandii* showed photosynthetic acclimation under elevated CO_2, and no photosynthetic down-regulation was observed in *G. biloba* and *P. tabulaeformis* [9].

In addition, down-regulation of photosynthesis in response to elevated CO_2 commonly involves a decrease in the chlorophyll content. However, in this study, no significant decrease in chlorophyll content was observed under elevated CO_2 (Fig. 2). This supported our findings that no significant down- regulation of photosynthesis in *G. biloba* and *P. tabulaeformis*.

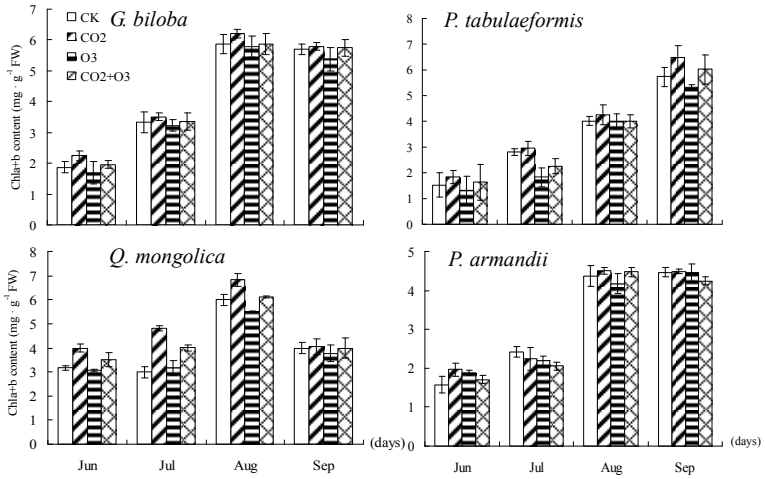

Fig. 2. Effects of elevated CO_2 and/or O_3 on chlorophyll (a+b) content in leaves of *G. biloba* and *Q. mongolica*, and previous-year needles of *P. tabulaeformis* and *P. armandii* in 2008. Data are means ± SE (n=9).

Our results showed that elevated O_3 decreased significantly Pn and g_s of every urban tree species, and decreased by 35.4% and 46.4%, 45.7% and 87.5%, 53.6% and 84.6%, 57.9% and 50% in maximum rate in Pn and g_s of *G. biloba, P. tabulaeformis, Q. mongolica and P. armandii*, respectively (Fig. 1 and 3).

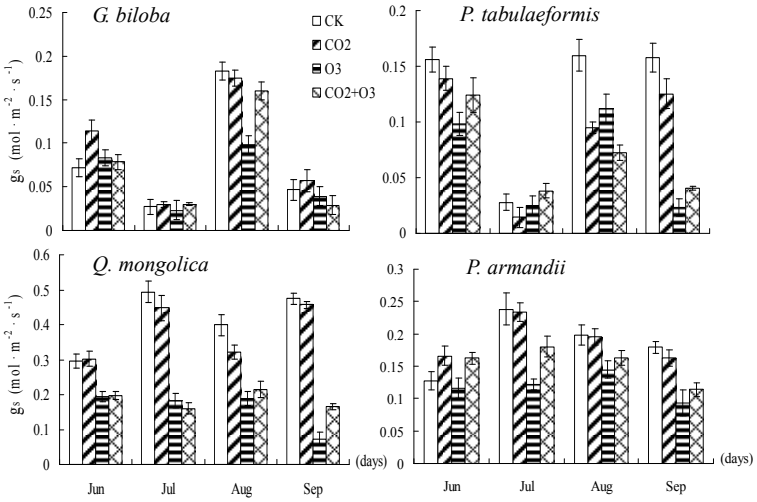

Fig. 3. Effects of elevated CO_2 and/or O_3 on stomatal conductance (gs) in leaves of *G. biloba* and *Q. mongolica*, and previous-year needles of *P. tabulaeformis* and *P. armandii* in 2008. Data are means ± SE (n=9).

Decline of photosynthesis was generally due to the stomotal factors in *G. biloba* leaves at the beginning of O_3 exposure. The differing sensitivity to O_3 among different plant species cannot be explained completely on the basis of uptake of the pollutant determined, in turn, by g_s. According to our results, elevated O_3 lead to loss of chlorophyll of every urban tree species. Loss of chlorophyll, leaf yellowing in other words, indicates that leaf senescence was accelerated by chronic O_3 fumigation. Higher decrease in chlorophyll content was observed in *Q. mongolica* than other tree species (Fig. 3). This also implied that *Q. mongolica* was more sensitive to elevated O_3.

Elevated CO_2 ameliorates the negative impact of elevated O_3 on photosynthesis in many plants. Our results showed that elevated CO_2 is able to totally or partly alleviate the harmful effects of elevated O_3 on trees. In addition, it also has been suggested that elevated CO_2 might reduce the

potential for oxidant damage, as has been tested by our recent studies [7], and elevated CO_2 ameliorated the accumulation of H_2O_2 induced by elevated O_3 in leaves of *G. biloba* [6].

Conclusion

Q. mongolica and *P. armandii* showed photosynthetic acclimation after long-term fumigation by elevated CO_2. *Q. mongolica* was more sensitive to elevated O_3 than *G. biloba*, and *P. tabulaeformis* than *P. armandii*. The combined effect of elevated CO_2 and O_3 caused the changes in photosynthetic parameters including Pn, gs and chlorophyll content that were more similar to ambient air (CK) or slightly lower than elevated CO_2, indicating that elevated CO_2 is able to totally or partly alleviate the harmful effects of elevated O_3 on urban tree species.

Acknowledgments

This research was supported by the National Natural Science Foundation of China (31170573, 31270518), and the National Natural Science Key Project (90411019).

References

[1] IPCC. Climate Change, "The physical scientific basis. Contribution of Working Group I to the Fourth Assessment Report of the Intergovernmental Panel on Climate Change (IPCC)," Cambridge University Press, Cambridge, UK, 2007, pp. 996.

[2] T.B. Ryerson, M. Frainer, J.S. Holloway, D.D. Parrish, L.G. Huey, D.T. Sueper, G.J. Forst, S.G. Donnelly, S. Schauffler, E.L. Atlas, W.C. Kuster, P.D. Goldan, G. Hubler, J.F. Meagher, F.C. Fehsenfeld, "Observations of ozone formation in plant plumes and implications for ozone control strategies," Sci. 272 (2001) 719-723.

[3] P. Antoni, A. Iker, B. Carmen, S. Robert, A.B. Joaquim, N. Salvador, "Effects of long-term exposure to elevated CO_2 conditions in slow-growing plants using a 12C-enriched CO_2-labelling technique," Rapid Commun. Mass Spectr. 23 (2009) 282-290.

[4] M. Kitao, M. Löw, C. Heerdt, T.E.E. Grams, K.H. Häberle, R. Matyssek, "Effects of chronic elevated ozone exposure on gas exchange responses of adult beech trees (*Fagus sylvatica*) as related to the within-canopy light gradient," Environ. Pollut. 157 (2009) 537-544.

[5] K. Bortier, R. Ceulemans, L. De Temmerman, "Effects of tropospheric ozone on woody plants," In: M. Agrawal, eds. Environmental pollution and plant responses. Lewis Publishers, Boca Raton, FL. 2000, pp. 153-182.

[6] T. Lu, X. He, W. Chen, "Effects of elevated O_3 and CO_2 on Pinus tabulaeformis antioxidant system," Chin. J. Ecol. 28 (2009) 1316-1323.

[7] K. Yan, W. Chen, X. He, G. Zhang, S. Xu, L. Wang, "Responses of photosynthesis, lipid peroxidation and antioxidant system in leaves of *Quercus mongolica* to elevated O_3," Environ. Exp. Bot. 69 (2010) 198-204.

[8] M. Liberloo, I. Tulva, O. Raim, O. Kull, R. Ceulemans, "Photosynthetic stimulation under long-term CO_2 enrichment and fertilization is sustained across a closed Populus canopy profile (EUROFACE)," New Phytol. 173 (2007) 537-549.

[9] N.T.D. Joseph, M.E. Kubiske, N. Nelson, K. Kets, J. Riikonen, A. Sober, L. Rouse, D.F. Karnosky, "Will photosynthetic capacity of aspen trees acclimate after long-term exposure to elevated CO_2 and O_3?," Environ. Pollut. 158 (2010) 983-991.

Advanced Materials Research Vols. 641-642 (2013) pp 26-29

doi:10.4028/www.scientific.net/AMR.641-642.26

Effect of Coal Dust on Coalbed Methane Wells Productivity

Hongze Ma[1, a]

[1]China University of Geosciences(Beijing), Beijing, China

[a]xiaowukong@yeah.net

Keywords: Coal dust; Permeability; CBM vertical well productivity

Abstract. CBM has the largest reserve except for conventional natural gas and is the cleanest energy. However, neither coal seam permeability nor CBM vertical well productivity has been determined when the immigration of coal dust are considered, which restricts the economic CBM exploitation. Based on coal seam characteristics, use permeability parallel path model and CBM seepage equation. The results show that with different ratio of non-clogging path and the total path, coal seam permeability and CBM vertical well productivity may either increase or decrease.

Introduction

Coal dust production is the phenomenon that coal dust immigrates from coal seam with fluids during the production of CBM. Most of CBM vertical wells productivity models are based on fluid-solid coupling method, but the calculation is rarely used in practice production. The article conducts a brief formula of steady-state CBM vertical wells productivity, which provides scientific base for the reasonable development of CBM.

The Maximum BHP with the Immigration of Coal Dust

The mechanism of the production of coal dust is that the coal seam tangential stress exceeds the coal particles cohesion, so the maximum flowing BHP when coal dust begins to immigrate is[1]:

$$p_{\max} = \rho g c_{\phi} H \cos\varphi\left(\frac{2\sigma}{1-\sigma} - b\right) - c \tag{1}$$

Model of Coal Dust Production Prediction

Coal Dust Curve. According to statistic data of coal dust production of many CBM wells, analyze the relationship between coal dust production and time through curve fit. Typical coal dust curve is showed in Fig. 1.

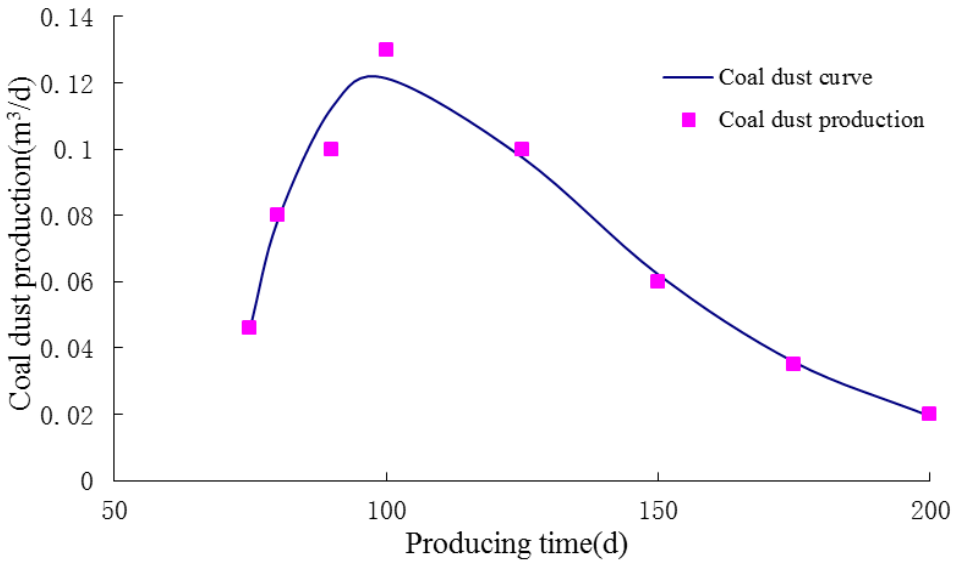

Fig. 1 Typical coal dust curve

Model of Coal Dust Production Prediction. Based on coal dust curve, the relationship between coal dust production and time obey approximately Gamma Distribution[2]:

$$q_s(t) = \frac{S\lambda^a}{\Gamma(a)}(t-t_0)^{a-1}e^{-\lambda(t-t_0)} \tag{2}$$

Make liner correction of pressure factor to Eq.2. The accumulated production of coal dust $Q_s(t)$ at time t is:

$$Q_s(t) = \int_{t_0}^{t} \alpha \frac{p_{\max} - p_{wf}}{p_i - p_0} \frac{S\lambda^a}{\Gamma(a)}(t-t_0)^{a-1}e^{-\lambda(t-t_0)}dt \tag{3}$$

Change of the Reservoir Physical Parameters after the Immigration of Coal Dust

Change of Permeability. Gruesbeck and Collins[3] proposed the concept of parallel path model. According to parallel path model:

$$k = \begin{cases} fk_0 e^{\left(\frac{\phi-\phi_0}{1-\phi_0}\right)} + (1-f)k_0 e^{(-\beta C_p^{\eta})}, & p_{wf} \le p_{\max} \\ k_0, & p_{wf} > p_{\max} \end{cases} \tag{4}$$

Assume that every coal dust particle has same size. The ratio of the volume of coal dust particles that plug pore and the volume of coal dust particles that immigrate out of the formation is (1-f)/f. So C_p is :

$$C_p = \frac{Q_s(t)}{\phi\pi h r_e^2}\frac{1-f}{f} \tag{5}$$

When the coal dust production is steady, the permeability is:

$$k|_{t=\infty} = fk_0 e^{\frac{\alpha S(p_{\max}-p_{wf})}{\pi r_e^2 h(p_i-p_0)(1-\phi_0)}} + (1-f)k_0 e^{-\beta[\frac{\alpha S(p_{\max}-p_{wf})}{\pi r_e^2 h\phi_0(p_i-p_0)}]^\eta} \tag{6}$$

The CBM Vertical Well Productivity Formula

Seepage Equation and Boundary Conditions. Considering the condition of CBM seepage in coal seam, the governing equation in a cylindrical coordinate is[4]:

$$\frac{1}{r}\frac{\partial}{\partial r}(r\frac{p}{\mu Z}\frac{\partial p}{\partial r}) = \frac{p_{sc}T}{kT_{sc}}q_v \tag{7}$$

Because all the CBM is desorbed from the coal matrix, Eq.7 is changed into:

$$\frac{1}{r}\frac{\partial}{\partial r}(rp\frac{\partial p}{\partial r}) = \frac{p_{sc}T\mu Z}{kT_{sc}}\frac{q}{\pi r_e^2 h} \tag{8}$$

Interior boundary condition is invariable output:

$$r\frac{\partial p}{\partial r}|_{r=r_w} = \frac{p_{sc}T}{pT_{sc}}\frac{\mu Z}{2\pi kh}q \tag{9}$$

Solution of the Equation. Integrate on both sides of Eq.8 and use boundary condition Eq.9, CBM vertical well productivity formation can be deduced:

$$p_e^2 - p_{wf}^2 = \frac{q\mu Z}{\pi hk}\frac{p_{sc}T}{T_{sc}}(1-\frac{r_e^2}{r_w^2})(\ln\frac{r_e}{r_w}+\frac{1}{2}) \tag{10}$$

Results and Analysis

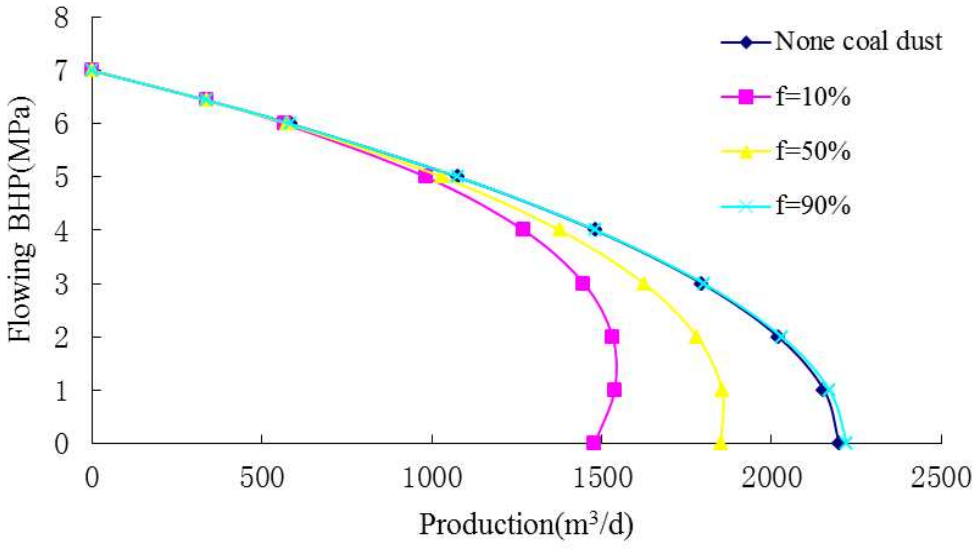

Fig. 2 CBM vertical well IPR curve with different value of f

Fig. 2 shows that with different value of f, the permeability may either increase or decrease. And because of the effect of coal dust, the CBM vertical wall production does not always increase with the decrease of flowing BHP.

Summary

1. The changing trend of permeability is associated to the coal seam pore structure. With different value of f, the permeability may either increase or decrease.
2. There is an inflection point in the IPR curve and the maximum production reaches at the inflection point. The value of f should be measured based on experiment for different coal seam to determine whether the CBM well should produce less coal dust or produce proper amount of coal dust to earn the maximal economic profit.

References

[1] Z.B. Yang: Southern China Oil & Gas, Vol. 16(2003), p. 59

[2] Y.Y. Luo, C.L. Li and S.J. Huang: Oil Drilling & Production Technology, Vol. 31(2009), p. 66

[3] D.S. Wang: *Manual of modern reservoir fracture-acidising technology* (Beijing Petroleum Industry Press, China 2006).

[4] Y.T. Shang: *Study on percolation mechanism and deliverability evaluation of CBM* (MS., China University of Petroleum, China 2008).

Advanced Materials Research Vols. 641-642 (2013) pp 30-34
© (2013) Trans Tech Publications, Switzerland
doi:10.4028/www.scientific.net/AMR.641-642.30

Heterogeneous Fenton System Dynamic Decolorization of Simulated Dye Wastewater

Yanjie Bi[1,3, a], Yukun Ma[2,3,b], Shengliang Zheng[2,3,c], Binsong Wang[2,3,d*]

[1] Financial Department, Heilongjiang University, Harbin 150080, China

[2] School of Chemistry and Materials Science, Heilongjiang University, Harbin 150080, China

[3] Key Laboratory of Functional Inorganic Material Chemistry, Ministry of Education and Key Laboratory of Environment-friendly Chemical Technology, College of Heilongjiang Province, Harbin 150080, China

[a]biyanjie@hlju.edu.cn, [b] 316901771@qq.com, [c] 105741861@ qq.com, [d]wangbinsong@hlju.edu. cn

[*]Corresponding author.E-mail: wangbinsong@hlju.edu. cn

Keywords: Heterogeneous Fenton; Dye wastewater; Dynamic decolorization; Resin

Abstract. Using heterogeneous Fenton system dynamic method, a decolorization test was operated for three kinds of simulated dye wastewater (Reactive Red KE-3B, Reactive Yellow KE-4R and Reactive Blue KN-R). Through the single factor experiments to examine the pH, H_2O_2 dosage, catalyst dosage, reaction temperature and residence time of simulated dye wastewater effected on the simulated dye wastewater decolorization rate. Determined the best decolorization reaction conditions as pH value of 4, the H_2O_2 concentration of 800 mg/L, catalyst dosage of 20 g, reaction temperature of 60 °C and reaction residence time of 9 minutes. Under this reaction conditions, in heterogeneous fenton system, degradation rate of the three kinds of simulated wastewater reached 95.01%, 93.86% and 97.74%, respectively.

Intorduction

Dye wastewater, containing dyes, dye auxiliaries, surface active agents, for its high chroma, low BOD/COD value (generally less than 0.2) and poor biodegradability[1], is hard to be treated. The advanced oxidation processes (AOPs) can generate hydroxyl radicals (·OH) in situ, a highly powerful oxidizing agent, and are effective in treatment of persistent organic pollutants in aqueous solutions until their overall mineralization[2]. Heterogeneous Fenton system as the main AOPs technology, with the ability to reuse the catalyst to improve the utilization rate of hydrogen peroxide, to broaden the reaction pH conditions, and effective solve the problem of secondary pollution generated in the homogeneous Fenton system reaction process, reduce the cost of recovering the iron sludge[3, 4]. Heterogeneous Fenton catalyst also has some drawbacks.[5-7]To solve these problems, our research group prepared heterogeneous Fenton system catalyst, without stirring during the reaction, to adequate protect the mechanical strength of the catalyst, and improve the cycle life of the catalyst and catalyst efficiency.

In this study, three kinds of reactive dyes were picked for the decolorization experimental study: Reactive Red KE-3B, Reactive Yellow KE-4R and Reactive Blue KN-R. The optimum reaction conditions of heterogeneous Fenton system were investigated under different pH, temperature, catalyst dosage, and H_2O_2 dosage and reaction residence time.

Experiment Section

Difference between the decolorization rate of Resin D072 and H_2O_2. A blank experiment shows that no decolorization effect without H_2O_2 dosing, H_2O_2 and pure resin D072 cannot constitute a heterogeneous Fenton system, and cannot decolorize three simulated dye wastewater. The degradation of heterogeneous Fenton system is mainly contributed by the catalyst strong oxidizing hydroxyl radicals which produced by the reaction between Fe^{2+} and H_2O_2, using the catalyst or H_2O_2 or resin D072 alone will not constitute a heterogeneous Fenton system, Unable to achieve the effect of degradation simulated dye wastewater.

The affecting of initial pH value on decolorization rate. Fixed reaction conditions: catalyst dosage of 20 g, the solution concentration of 400 mg/L, three kinds of simulated dye wastewater solutions 1L, H_2O_2 dosage of 800 mg/L, the dye solution temperature of 60 °C and the reaction residence time of 9 min, to investigate the initial pH value 3, 4, 5, 6 and 7 of the heterogeneous Fenton system that effect decolorization rate of the three kinds of simulated dye wastewater, the experiment al results shown in Fig. 1.

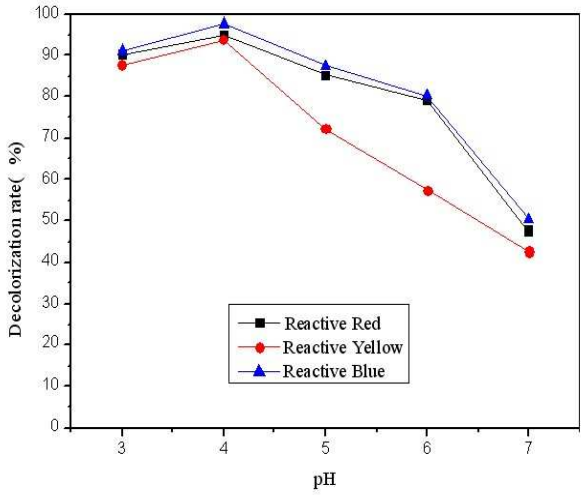

Fig. 1 Effect of initial pH on decoloration rate of three kinds of dyes

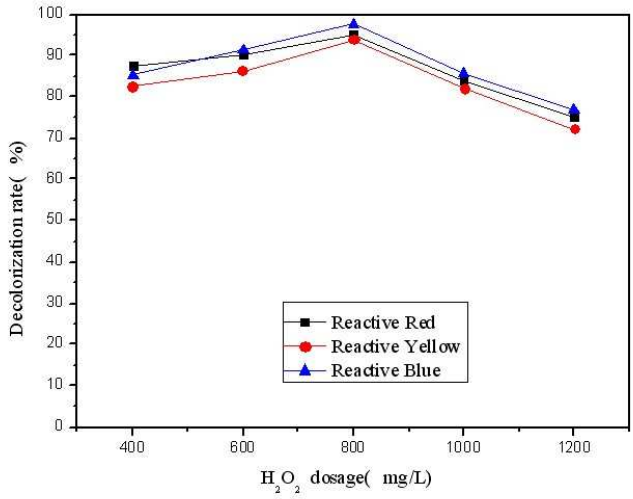

Fig. 2 Effect of H_2O_2 doses on decoloration rate

Fig. 1 shows that, when initial pH of 3, the decolorization rate of three kinds of simulated dye wastewater were 90.31%, 87.73% and 91.14%, respectively. With the increase of the initial pH, the decolorization rate is gradually increasing. When initial pH of 4, the decolorization rate of three simulated dye wastewater were 97.74%, 95.01% and 93.86%, reached maximum. Since then, as the initial pH of the solution continue to increase, decolorization rate of three simulated dye wastewater is significantly reduced. When the initial pH value increased to 7, decolorization rate of three kinds of simulated dye wastewater dropped to 47.52%, 42.58% and 50.36%, respectively. At high pH value, adsorbed Fe^{2+} is readily oxidized as of Fe^{3+} and Fe^{3+} easily hydrolyzed to form a flocculent precipitate Fe $(OH)_3$, so that the solution of the Fe^{2+} concentration decreased, resulting in the decrease of the decolorization rate. When pH of 3, higher H^+ concentration cause a inhibition of hydroxyl radical generation, oxidative degradation affect the heterogeneous Fenton system, thereby affecting the decolorization rate. Therefore, selected pH of 4 as the best pH value for heterogeneous Fenton system dynamically degradation of simulated dye wastewater.

The affecting of H_2O_2 dosage on decolorization rate. Fixed reaction conditions: catalyst dosage of 20 g, the solution concentration of 400 mg/L, three kinds of simulated dye wastewatersolutions 1 L, initial pH of 4, the dye solution temperature of 60 °C and the reaction residence time of 9 min, investigate the impact of different H_2O_2 dosage(400,600,800,1000 and 1 200 mg/L) to the decolorization rate of three simulated dye wastewater, results shown in Figure.2

Fig. 2 shows when H_2O_2 dosage of 400 ~ 800 mg/L, the decolorization rate of three kinds of simulated dye wastewater and the H_2O_2 dosage positively correlated. H_2O_2 dosage of 800 mg/L the decolorization rate of simulated dye wastewater reached their maximum(95.01%, 93.86 % and 97.74%). When H_2O_2 dosage morer than 800 mg/L the decolorization rate of three simulated dye wastewater was significantly reduced with the increasing of H_2O_2 dosage. When H_2O_2 dosage is increased to 1200 mg/L, the decolorization rate of three kinds of simulated dye wastewater was reduced to 75.34%, 72.27% and 76.91%. This is due to the small dosage of H_2O_2, lack of hydroxyl radicals which Fe^{2+} react with H_2O_2, cannot meet the needs of the oxidative degradation reaction conditions of heterogeneous Fenton system. H_2O_2 excessive dosing solution will generate too much HO_2 • (H_2O_2 + • OH → HO_2 • + H_2O, HO_2 •), the oxidative capacity of HO_2 • is weaker than H_2O_2, the decolorization rate of simulated dye wastewater decreased. Therefore, the optimum dosage of H_2O_2 for heterogeneous Fenton system dynamically degradation of simulated dye wastewater is 800mg • L^{-1}.

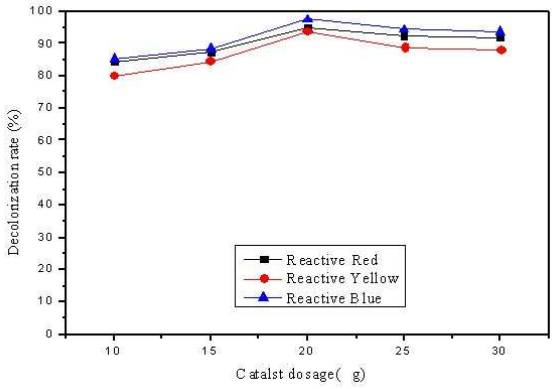

Fig. 3 Effect of different catalyst adding amount on decoloration rate

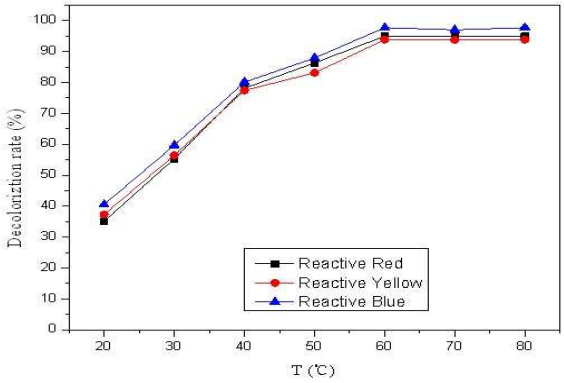

Fig. 4 Effect of different tempretures on decoloration rate

The affecting of catalyst dosage on decolorization rate. Fixed reaction conditions: H_2O_2 dosage was 800 mg/L, the solution concentration of 400 mg/L, three kinds of simulated dye wastewater solutions 1 L, initial pH of 4, the dye solution temperature of 60 ° C and the reaction residence time of 9 min, investigate the impact of different catalyst dosage (10, 15, 20, 25 and 30 g) to the decolorization rate of three simulated dye wastewater, as shown in Fig. 3.

Fig. 3 shows with the catalyst dosage of 10 g, the decolorization rate of three kinds of simulated dye wastewater were 84.51%, 80.17%and 85.42%. Catalyst dosage increased from 10 g to 20 g, the decolorization rate increased with the increasing of catalyst dosage. When the catalyst dosage of 20 g, the decolorization rate three kinds of simulated dye wastewater reaches the maximum value 95.01%, 93.86% and 97.74%, respectively. Due to the non-selective reaction of the hydroxyl radical, when the catalyst dosage is excessive, the Fe^{2+} direct reacted with hydroxyl radicals, consuming part of the hydroxyl radicals generated, so that within the same reaction time in the reaction system the decrease in the amount of hydroxyl radicals, lead to decolorization rate reduced. The best catalyst dosage of Heterogeneous Fenton system dynamic degradation of simulated dye wastewater is 20 g.

The affecting of dye solution temperature on decolorization rate. Fixed reaction conditions: catalyst dosage of 20 g, the solution concentration of 400 mg/L, three kinds of simulated dye wastewater solutions 1L, initial pH of 4, the reaction residence time of 9 min and H_2O_2 dosage to

800 mg/L, investigate the impact of different dye solution temperature (20, 30, 40, 50, 60, 70 and 80 °C) to the decolorization rate of three simulated dye wastewater, as shown in Fig. 4.

Fig. 4 shows, reaction temperature of 20 °C, the decolorization rate of three kinds of simulated dye wastewater were low and did not exceed 40%. As the temperature increased, the decolorization rate increased, when the temperature raised to 60 °C, the decolorization rate increased to 95.01%, 93.86% and 97.74% respectively, have reached their maximum. This is due to the with reaction temperature elevating, the reactant molecules absorbing heat, increasing the activation energy of the reactants, thereby increasing the frequency of collision between the reactants, accelerating the rate of the decolorization reaction. The best solution temperature of simulated dye wastewater is 60 °C.

The affecting of reaction residence time on decolorization rate. Fixed reaction conditions: catalyst dosage of 20 g, the solution concentration of 400 mg/L, three kinds of simulated dye wastewater solutions 1 L, initial pH of 4, the solution temperature of 60 °C and H_2O_2 dosage to 800 mg/L, investigate the impact of different different reaction residence time (3, 6, 9, 12 and 15 min) to the decolorization rate of three simulated dye wastewater, as shown in Fig. 5.

Fig. 5 shows that when the reaction residence time of simulated dye wastewater is less than 9 min, decolorization rate of simulated dye wastewater increasing with the residence time of the reaction increased. With the residence time of 9 min, decolorization rate of simulated dye wastewater reached their maximum value of 95.01%, 93.86 and 97.74%, respectively. Increasing of residence time, a small amount of the catalyst Fe^{2+} which resolved to the solution, Fe^{2+} was oxidized to Fe^{3+} (color of yellow), so decolorization rate of dye Reactive Yellow reduced. The best reaction residence time of Heterogeneous Fenton system dynamic degradation of simulated dye wastewater is 9 min.

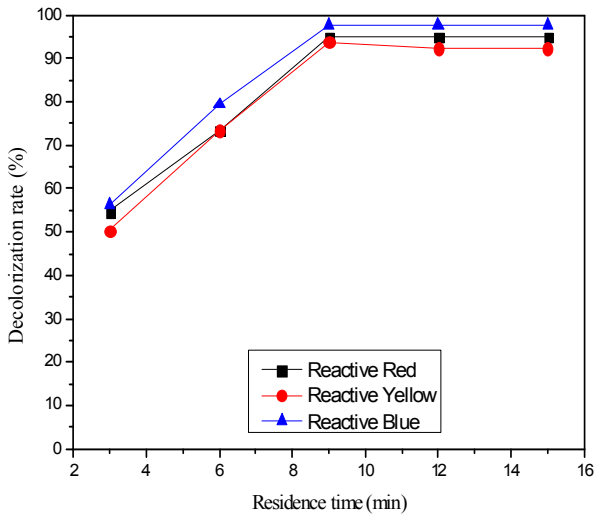

Fig. 5 Effect of different stay time on decoloration rate

Summary

The efforts on heterogeneous Fenton system have showed great improvement on the progress of catalyst development by using a lesser amount of oxidizing agent, wide range of reaction pH, higher catalytic activities and encouraging kinetic rate compared to homogenous catalyst. Here we discussed the decolorization of simulated dye wastewater using heterogeneous Fenton system dynamic method. Determined the best decolorization reaction conditions as pH value of 4, the H_2O_2 concentration of 800 mg/L, catalyst dosage of 20 g, reaction temperature of 60 °C and reaction residence time of 9 minutes. Under this reaction conditions, degradation rate of the three kinds of

simulated wastewater reached 95.01%, 93.86% and 97.74% respectively. That shows an excellent degradation property of our resin loading heterogeneous Fenton system which have a good prospect of application in the field of dye wastewater treatment.

Acknowledgements

This work was financed by Fundamental Research Funds for the Central Universities(DL11CA01), Youth Science and Technology Innovation Fund of Harbin (RC2012QN002074) and Heilongjiang Postdoctoral Science-Research Foundation(LBH-Q11011).

References

[1] S.C.R.Santos, V.J.P. Vilar, R.A.R. Boaventura, Waste metal hydroxide sludge as adsorbent for a reactive dye, J. Journal of Hazardous Materials. 153 (2008) 999-1008.

[2] E. Rosales, Electro-Fenton decoloration of dyes in a continuous reactor: A promising technology in colored wastewater treatment. Chemical Engineering Journal, J. 155 (2009). 62-67.

[3] H. Kušić, N. Koprivanac, I. Selanec, Fe-exchanged zeolite as the effective heterogeneous Fenton-type catalyst for the organic pollutant minimization: UV irradiation assistance, J. Chemosphere. 65 (2006) 65-73.

[4] Y. Zhao, J. Hu, W. Jin, Transformation of oxidation products and reduction of estrogenic activity of 17β-Estradiol by a heterogeneous photo-Fenton reaction, J. Environmental Science & Technology. 42 (2008) 5277-5284.

[5] G.B. Ortiz de la Plata, O.M. Alfano, A.E. Cassano, Decomposition of 2-chlorophenol employing goethite as Fenton catalyst. I. Proposal of a feasible, combined reaction scheme of heterogeneous and homogeneous reactions, J. Applied Catalysis B: Environmental. 95 (2010) 1-13.

[6] G.B. Ortiz de la Plata, O.M. Alfano, A.E. Cassano, Decomposition of 2-chlorophenol employing goethite as Fenton catalyst II: Reaction kinetics of the heterogeneous Fenton and photo-Fenton mechanisms, J. Applied Catalysis B: Environmental. 95 (2010) 14-25.

[7] W. Wang, Novel NaY zeolite-supported nanoscale zero-valent iron as an efficient heterogeneous Fenton catalyst, J. Catalysis Communications. 11 (2010) 937-941.

Advanced Materials Research Vols. 641-642 (2013) pp 35-38

doi:10.4028/www.scientific.net/AMR.641-642.35

Action of flow Rate of Mobile Phase in Chromatography

Zhang Dali [1, a], Ke Jiajun[2], Lu Lizhu[2]

[1] Biochemical Engineering College, Beijing Union University, Beijing, China

[2] Institute of Process Engineering, Chinese Academy of Science, Beijing, China

[a] Email: dali@buu.edu.cn (corresponding author)

Keywords: chromatography; flow rate; mobile phase; plate number; plate theory; slip mechanism

Abstract. Chromatography has found an increasingly wide utilization in scientific and technological fields, even in some cases, has become indispensable methods for analysis and separation. Compared with its application, some common queries in chromatography still lack for good theoretical explanations, for instance, the action of flow rate of mobile phase on symmetry of peak. As is familiar to people, an increase in flow rate of mobile phase always causes theoretical plate number to decrease under normal conditions. At the same time, maybe the symmetry of chromatographic peak obviously increases, on the contrary. This result is self-contradictory. Why does the theoretical plate number not increase under the condition? Utilizing our prior paper on five plate numbers in chromatography, this paper points out why theoretical plate number decreases with an increase in symmetry of peak when flow rate of mobile phase increases. Based upon gas-solid chromatography results, the relation between flow rate of mobile phase and frequency of partition of solute, and the relation between flow rate and plate number are deduced. From the angle of theoretical model, this paper discusses the relation between solute partition in static mobile phase such as partition between two phases in plate theory and solute partition in flowing mobile phase such as Martin-Synge partition in slip mechanism, and their characteristics.

Introduction

Why does plate number not increase at the time when the symmetry of chromatographic peak obviously increases?, and what is the effect of flow of mobile phase on plate number?, they are the questions which will be discussed and answered in this paper.

1. Experiments

Chromatograph: Shimadzu GC-14C. N2000 chromatographic work station of Zhejiang University; stationary phase：GDX-101; column: three meters; column temperature: 180℃; mobile phase: N_2; flame ionization detector; solutes: *n*-pentane, *n*-hexane, cyclohexane, *n*-heptane and isooctane, analytical reagents. The five solutes in equal volume are mixed, as a sample;. Chromatogram is converted into text file in data output. The output data of peak are fitted with the elution curve equation of slip mechanism through software origin6.0, and the value of parameters in the equation can be gotten. Flow rate of mobile phase (carrier gas) is represented by the gage pressure of carrier gas at inlet of column, in this paper.

2. Properties of Five Plate Numbers

Calculations of Five Plate Numbers. The relational expressions of five plate numbers derived in our prior paper [1] are as follows.

theoretical plate number: $n_0 = 5.54\left(t_R / W_{1/2}\right)^2$. (1)

real plate number: $n = 5.54\left(t_R / W_{1/2}\right)^2 \left(k/(1+k)\right)$. (2)

plate-model plate number: $q_o \approx n$ [2]. (3)

slip plate number: $q = 5.54\left(t_R / W_{1/2}\right)^2 \left(k/(1+k)\right)\left(1 - c_t / t_R\right)$. (4)

peak plate number: $q' = 5.54\left(t_R / W_{1/2}\right)^2 \left(k/(1+k)\right)\left(1 - c_t / t_R\right)^2$. (5)

t_R is retention time, $W_{1/2}$ is half peak width, k is partition ratio, c_t is apparent slip factor and can be known through experimental elution curve fitting to equation (6), which is the elution curve equation of slip mechanism[1].

$$Y(t) = Y_0 + \frac{A\sqrt{B}}{\sqrt{2\pi} \times \sqrt{(t - c_t)}} e^{-\frac{B(t_{nR} - t)^2}{2(t - c_t)}} \quad (6)$$

Properties of Five Plate Numbers. Figure 1 shows the relation between several plate numbers and flow rate of mobile phase. As revealed from Figure 1, an increase in flow rate of mobile phase makes theoretical plate number, real plate number decrease, and slip plate number, peak plate number increase

Partition ratio k can be regarded as a constant due to constant temperature and just a change in flow rate. According to equation (1) and equation (2), theoretical plate number and real plate number change just with the ratio of retention time to half peak width, ($t_R/w_{1/2}$). The ($t_R/w_{1/2}$) is independent of symmetrical characteristic of peak, and generally decreases with an increase in flow rate of mobile phase. So that theoretical plate number is independent of symmetrical characteristic of peak, and generally decreases with an increase in flow rate of mobile phase.

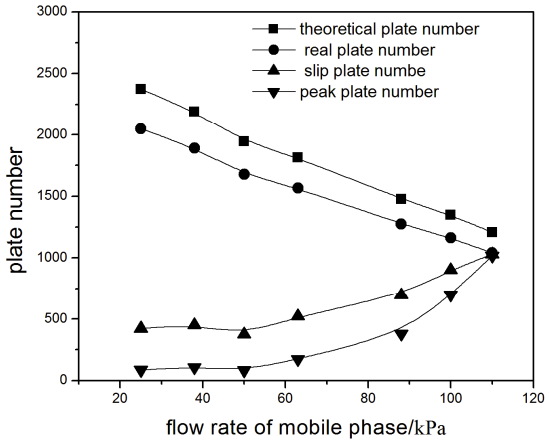

Figure 1 Chromatographic properties of *n*-hexane as solute

*The flow rate of mobile phase is expressed by kPa: gage pressure of carrier gas at inlet of column

According to equation (4), slip plate number relates not only to ($t_R/w_{1/2}$) but also to ($1\text{-}c_t/t_R$). The ($1\text{-}c_t/t_R$) relates closely to symmetry of peak and increases with the increase of symmetry of peak. As a result, when flow rate of mobile phase increases, the symmetry of peak increases, ($1\text{-}c_t/t_R$) also increases, finally, though （$t_R/w_{1/2}$）decreases, but slip plate number increases.

3. Relation between Flow Rate and Plate Number

Compared with slip plate number, theoretical plate number loses the important information of system: symmetrical characteristic of peak. So the following discussion merely is about the relation between flow rate and slip plate number.

As shown in figure 1, an increase in flow rate of mobile phase leads to the increase of slip plate number, the cause of which obviously is the acceleration of partition of solute, the increase of frequency of partition. The frequency of partition is the number of times per unit time for partition of solute occurring. The unit time usually is minute in chromatography.

The acceleration of partition of solute naturally is the result of molecular collision of mobile phase to solutes. According to collision law in physics, collision between bodies can lead to energy transfer. Therefore, it can be deemed that molecular collision of mobile phase to solutes leads to energy transfer and solute molecules obtain energy, so that solute partition is accelerated.

Relation between Flow Rate and Partition Frequency. (a)when flow rate of mobile phase increases, move rate of molecule of mobile phase increases, and kinetic energy of molecule of mobile phase increases, and the energy transmitted by collision increases.

Suppose: when flow rate increases, the increase in partition energy obtained by solute ($\Delta E_{\text{partition}}$) is in direct proportion to the increase of kinetic energy of molecule of mobile phase ($\Delta E_{\text{kinetic}}$), due to molecular collision between mobile phase and solute.

$$\Delta E_{partition} = k_1 \Delta E_{kinetic}. \quad (7)$$

k_1 is scale coefficient.

(b) The increase of partition energy obtained by solute will lead to acceleration of partition motion of solute. Suppose: when the increases of partition energy is a certain quantity, the partition of solute will accelerates according to a certain ratio, so frequency of partition of solute (f) increases according to a certain ratio. For instance, the ratio of increase for frequency of partition is 20%. Therefore the ratio of increase of partition frequency ($\Delta f/f$) should be in direct proportion to the increase of partition energy ($\Delta E_{partition}$)

$$\Delta f/f = k_2 \Delta E_{partition}. \quad (8)$$

(c) Suppose: before the increase of flow rate of mobile phase, the kinetic energy of mobile phase molecule which collides with solute is $(1/2)m(v_1)^2$; after the increase of flow rate, the kinetic energy this moment is $(1/2)m(v_2)^2$;

$v_2 = v_1 + k_3\Delta v$.

Δv is the increment of linear rate of mobile phase throughout the increase of flow rate. k_3 is a scale coefficient. The increment of kinetic energy of mobile phase molecule is $\Delta E_{kinetic}$.

$$\Delta E_{kinetic} = (1/2)m(v_1+k_3\Delta v)^2 - (1/2)m(v_1)^2$$
$$= (1/2)m((v_1+k_3\Delta v)^2 - (v_1)^2)$$
$$= (1/2)m\, k_3\, (k_3(\Delta v)^2 + 2\, v_1 \Delta v).$$

if $v_1 >> \Delta v$, $2v_1\Delta v >> (\Delta v)^2$. If k_3 is not large, the term $k_3(\Delta v)^2$ in the above equation can be neglected.

$$\Delta E_{kinetic} = k_3 m v_1 \Delta v. \quad (9)$$

v_1 belongs to rate of heat motion of gaseous molecule. Even if at ordinary temperature, v_1 is generally at least several hundred meters per second. So that v_1 far exceeds the linear rate of flow of mobile phase.

Equation (7) and equation (9) are substituted in equation (8) in turn, which results in equation (10).

$$\Delta f/f = k_1 k_2\, k_3 m v_1 \Delta v. \quad (10)$$

(d) The linear rate of flow of mobile phase (v) has linear relationship with gage pressure of carrier gas at inlet of column (p), therefore the increment of the linear rate (Δv) is in direct proportion to the increment of the gage pressure (Δp).

$$\Delta v = k_4 \Delta p. \quad (11)$$

Equation (11) is substituted in equation (10), which results in equation (12).

$$\Delta f / f = k_1 k_2\, k_3\, k_4 m\, v_1 \Delta p. \quad (12)$$

Given: $k_5 = k_1 k_2 k_3 k_4\, m\, v_1$.

$$\Delta f / f = k_5 \Delta p. \quad (13)$$

$$df/f = k_5 dp. \quad (14)$$

Integrating equation (14) results in equation (15).

$$ln(f) = k_5 p + c. \quad (15)$$

$c = ln(f_0)$, when column temperature is invariant (k_5 is invariant) and $p = 0$. The f_0 corresponds to the partition frequency of solute on the condition where gage pressure of carrier gas at inlet of column is zero, at given column temperature.

$$ln(f) = k_5 p + ln(f_0).$$

$$f = f_0 \exp(k_5 p). \quad (16)$$

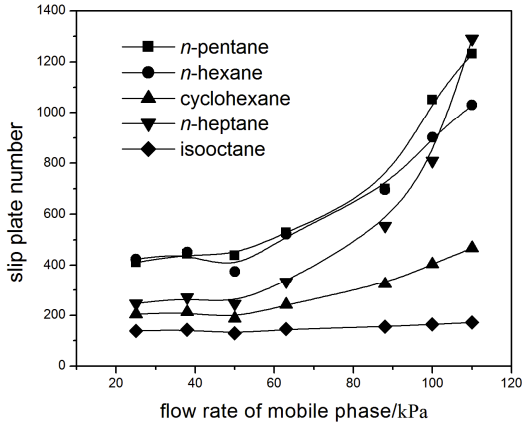

Figure 2 Relation between slip plate number and flow rate of mobile phase